

Ocean Colour Multi-Mission Algorithm Prototype System (OMAPS)

Algorithm Theoretical Baseline Document - System Vicarious Calibration

Ref: D2.1.1
Date: 29/07/2021
Issue: 1.2
For: EUMETSAT

Table of Contents

Table of Contents	2
Document Control	3
Applicable Documents	3
Reference Documents	3
List of Acronyms	7
1 Introduction.....	9
1.1 Scope of the document	9
1.2 Context of SVC.....	9
1.3 Reminder of the standard method	10
1.4 Challenge of SVC for non-standard AC	12
1.5 Generalising the SVC definition	13
2 Algorithm description	15
2.1 Processing outline	15
2.2 Algorithm input	16
2.2.1 In situ data	16
2.2.2 EO data and match-ups	16
2.2.3 OC processor.....	16
2.3 Theoretical description	18
2.3.1 Data screening	18
2.3.2 Sensitivity of AC	18
2.3.3 SVC in the VIS.....	19
2.3.4 SVC in the NIR	22
2.3.5 Mission average gain	22
2.4 Algorithm output.....	22
2.5 Performance estimates	23
2.6 Practical considerations.....	25
2.7 Results.....	25
2.7.1 Case studies and configurations	25
2.7.2 POLYMER/OLCI-A.....	26
3 Assumption and limitations.....	39

Document Control

Version No.	Release Date	Author/Contributor	Reason for issue
1.0	02/12/19	C. Mazeran (SOLVO)	Initial draft version
1.1	04/02/20	C. Mazeran (SOLVO)	Sections 2.1, 2.3.3, 2.4 and 2.6 completed
1.2	29/07/21	C. Mazeran (SOLVO)	Section 2.2 updated and 2.7 fully rewritten with results for POLYMER & SACSO

Applicable Documents

ID	Document
AD-1	EUMETSAT General SoW
AD-2	EUMETSAT Specific SoW for ocean colour prototype
AD-3	ID 995318 Level 2 Product Monitoring –Evolution Studies Multi-mission Ocean Colour (OC) Prototyping algorithm – PML Proposal
AD-4	OMAPS deliverable D1.1 Requirement Baseline for Offline Processor

Reference Documents

Antoine D. and Morel A. (1999). A multiple scattering algorithm for atmospheric correction of remotely-sensed ocean colour (MERIS instrument): principle and implementation for atmospheres carrying various aerosols including absorbing ones. *Int. J. Rem. Sens.*, 20(9): 1875-1916.

Antoine, D., Guevel, P., Deste, J. F., Bécu, G., Louis, F., Scott, A. J., and Bardey, P. (2008). The “BOUSSOLE” buoy-a new transparent-to-swell taut mooring dedicated to marine optics: Design, tests, and performance at sea. *Journal of Atmospheric and Oceanic Technology*, 25, 968–989.

Bailey, S. W., and Werdell, P.J. (2006). A multi-sensor approach for the on-orbit validation of ocean color satellite data products. *Remote Sensing of Environment* 102, 12-23.

Bailey, S.W., Hooker, S. B., Antoine, D., Franz, B. A., and Werdell, P. J. (2008). Sources and assumptions for the vicarious calibration of ocean color satellite observations. *Applied Optics*, 47, 2035–2045.

Bailey, S. W., Franz, B. A. and Werdell, P. J. (2010). Estimations of near-infrared water-leaving reflectance for satellite ocean color data processing. *Opt. Express* 18(7), 7521–7527.

Baith, K., Lindsay, R., Fu, G. and McClain, C. R. (2001). Data analysis system developed for ocean color satellite sensors. *EOS. Trans. AGU* 82, 202.

Brewin, R. J. W., Mélin, F., Sathyendranath, S., Steinmetz, F., Chuprin, A., Grant, M. (2014). On the temporal consistency of chlorophyll products derived from three ocean-colour sensors. *ISPRS Journal of Photogrammetry and Remote Sensing*, 97, 171-184.

Bricaud, A., and Morel, A. (1987). Atmospheric corrections and interpretation of marine radiances in CZCS imagery: use of a reflectance model. *Oceanologica Acta*, N°SP, 33-50.

Brockmann, C., Ruescas, A., and Stelzer, K. (2011). OC-CCI Pixel Identification. ESA OC-CCI Algorithm Theoretical Basis Document ref. AO-1/6207/09/I-LG, Issue 1.

Brown, S.W., Flora, S.J., Feinholz, M.E., Yarbrough, M.A., Houlihan, T., Peters, D., Kim, Y. S., Mueller, J., Johnson, B.C., Clark, D.K. (2007). The Marine Optical BuoY (MOBY) radiometric calibration and uncertainty budget for ocean color satellite sensor vicarious calibration. *Proc. SPIE Optics and Photonics; Sensors, Systems, and Next-Generation Satellites XI*.

Chomko, R. M., Gordon, H. R., Maritoner, S., and Siegel, D. A. (2003). Simultaneous retrieval of oceanic and atmospheric parameters for ocean color imagery by spectral optimization: A validation. *Remote Sensing of Environment*, 84, 202–220.

Clark, D.K., Yarbrough, M. A., Feinholz, M. E., Flora, S., Broenkow, W., Kim, Y. S., Johnson, B. C., Brown, S. W., Yuen, M., and Mueller, J. L. (2003). MOBY, a radiometric buoy for performance monitoring and vicarious calibration of satellite ocean color sensors: Measurement and data analysis protocols, in *Ocean Optics Protocols for Satellite Ocean Color Sensor Validation, Revision 4, Volume VI: Special Topics in Ocean Optics Protocols and Appendices. NASA/TM-2003-211621/Rev4-Vol.VI:3-34, Greenbelt, MD*.

Cox, C., and Munk, W. (1954). Measurement of the roughness of the sea surface from photographs of the sun's glitter. *J. Opt. Soc. Am.* 44(11), 838-850.

Delwart, S. and Bourg, L. (2013). MERIS calibrations: 10 years. *Proc. SPIE 8866, Earth Observing Systems XVIII, 88660Y (September 23, 2013)*.

Doerffer, R. and Schiller, H. (2007). The MERIS Case 2 water algorithm. *International Journal of Remote Sensing*, 28, 517–535.

Doerffer, R. (2015). Level-2 processing of MERIS data of case 2 waters, ATBD of MERIS 4th reprocessing, issue no 2.

Eplee, R. E., Robinson, W. D., Bailey, S. W., Clark, D. K., Werdell, P. J., Wang, M., Barnes, R. A., McClain, C. R. (2001). Calibration of SeaWiFS. II. Vicarious techniques. *Applied Optics*, 40, 6701–6718.

Eplee, R. E., Jr., Sun, J. -Q., Meister, G., Patt, F. S., Xiong, X., & McClain, C. R. (2011). Cross calibration of SeaWiFS and MODIS using on-orbit observations of the moon. *Applied Optics*, 50, 120–133

Evans, R. H., and Gordon, H. R. (1994). CZCS 'System Calibration': a retrospective examination. *Geophys. Res.* 99C: 7293-7307.

Feng, H., Vandemark, D., Campbell, J. W., and Holben, B. N. (2008). Evaluation of MODIS ocean color products at a northeast United States coast site near the Martha's Vineyard Coastal Observatory. *International Journal of Remote Sensing*, 29, 4479–4497.

Franz, B. A., Bailey, S. W., Werdell, P. J., & McClain, C. R. (2007). Sensor-independent approach to the vicarious calibration of satellite ocean color radiometry. *Applied Optics*, 46, 5068–5082.

Frouin, R. and Pelletier, B (2015). Bayesian methodology for inverting satellite ocean-color data. *Remote Sensing of Environment*, 159: 332 –360.

Gordon, H. R. (1978). Removal of atmospheric effects from satellite imagery of the oceans. *Appl. Opt.* 17, 1631 –1636.

Gordon, H. R. (1987). Calibration requirements and methodology for remote sensors viewing the ocean in the visible. *Remote Sensing of Environment*, 22, 103–126.

Gordon, H. R. (1998). In-orbit calibration strategy for ocean color sensors. *Remote Sensing of Environment*, 63, 265-278.

Gordon, H. R. and Wang, M. (1994). Retrieval of water-leaving radiance and aerosol optical thickness over the oceans with SeaWiFS: A preliminary algorithm. *Appl. Optics*, 33: 443-452.

Hollmann, R., Merchant, C. J., Saunders, R., Downy, C., Buchwitz, M., Cazenave, A., Chuvieco, E., Defourny, P., De Leeuw, G., Forsberg, R., Holzer-Popp, T., Paul, F., Sandven, S., Sathyendranath, S., van Roozendaal, M., Wagner, W. (2013). The ESA Climate Change Initiative: satellite data records for essential climate variables. *Bulletin of the American Meteorological Society*, 94 (10), pp.1541-1552.

Hu, C., Feng, L., Lee, Z-P., Davis, C.O., Mannino, A., McClain, C.R., and Franz, B.A. (2012). Dynamic range and sensitivity requirements of satellite ocean color sensors: learning from the past. *Applied Optics*, 51(25): 6045-6062.

Kuchinke, C. P., Gordon, H. R., and Franz, B. A. (2009). Spectral optimization for constituent retrieval in Case II waters I: Implementation and performance. *Remote Sensing of Environment*, 13, 571–587.

Lavender, S., Jackson, T. and Sathyendranath, S. (2015). The Ocean Colour Climate Change Initiative. *Ocean Chall.*, 21, 29–31.

Lebreton, C., Stelzer, K., Brockmann, C., Bertels, L., Pringle, N., Paperin, M., Danne, O., Knaeps, E., and Ruddick, K. (2016). Cloud and cloud shadow masking of high and medium resolution optical sensors - an algorithm inter-comparison example for Landsat-8. *Proceedings of the 2016 ESA Living Planet Symposium held in Prague, Czech Republic, 9-13 May 2016, ESA Special Publication SP-740.*

Lerebourg, C., Mazeran, C., Huot, J., & Antoine, D. (2011). Vicarious adjustment of the MERIS ocean colour radiometry. *MERIS ATBD 2.24 issue 1.0.*

Maritorea S., O. Hembise Fanton d’Andon, A. Mangin, and D.A. Siegel. (2010). Merged Satellite Ocean Color Data Products Using a Bio-Optical Model: Characteristics, Benefits and Issues. *Remote Sensing of Environment*, 114, 8: 1791-1804.

Mazeran et al., 2017: Requirements for Copernicus Ocean Colour Vicarious Calibration Infrastructure. Eumetsat contract EUM/CO/16/4600001772/EJK

Mazeran, C., Brockmann, C., Ruescas, A., Steinmetz, F. (2019). System Vicarious Calibration of SeaWiFS, MODIS, MERIS and VIIRS sensors processed by POLYMER. *ESA OC-CCI ATBD, v1.0.*

Mazeran, C., Ruescas, A. (2020). Ocean Colour System Vicarious Calibration Tool: Tool Documentation (DOC-TOOL). EUMETSAT report ref. EUM/19/SVCT/D2, available at <https://www.eumetsat.int/ocean-colour-system-vicarious-calibration-tool>.

Mélin, F., G. Zibordi, and S. Djavidnia (2009). Merged series of normalized water leaving radiances obtained from multiple satellite missions for the Mediterranean Sea. *Adv. Space Res.* 43, 423–437.

Mélin, F. and Giuseppe Zibordi (2010). Vicarious calibration of satellite ocean color sensors at two coastal sites. *Applied Optics*, 49, 798-810.

Morel, A., and Gentili, B. (1996). Diffuse reflectance of oceanic waters. 3. Implication of bidirectionality for the remote-sensing problem. *Applied Optics*, 35, 4850-4862.

Morel, A., and Maritorena, S. (2001). Bio-optical properties of oceanic waters: A reappraisal. *Journal of Geophysical research*, 106, 7763-7780.

Morel, A., Antoine, D. and Gentili, B. (2002). Bidirectional reflectance of oceanic waters: Accounting for Raman emission and varying particle phase function, *Applied Optics*, 41, 6289-6306.

Mueller, L., Clark, D. K., Kuwahara, V. S., Lazin, G., Brown, S., Fargion, G. S., Yarbrough, M. A., Feinholz, M., Flora, S., Broenkow, W., Kim, Y. S., Johnson, B. C., Yuen, M., Strutton, P. G., Dickey, T. D., Abbott, M. R., Letelier, R. M., Lewis, M. R., McLean, S., Chavez, F. P., Barnard, J. R. M. A., Subramaniam, A., Manov, D., Zheng, X., Harding, J. L. W., Barnes, R. A., and Lykke, K. R. (2003). Ocean optics protocols for satellite ocean color sensor validation, Revision 4, Volume VI: Special topics in ocean optics protocols and appendices. NASA/TM-2003-211621/Rev4-Vol.VI, Greenbelt, MD.

Müller, D., Krasemann, H., Brewin, R. J. W., Brockmann, C., Deschamps, P.-Y., Doerffer, R., Fomferra, N., Franz, B. A., Grant, M. G., Groom, S. B., Mélin, F., Platt, T., Regner, P., Sathyendranath, S., Steinmetz, F., Swinton J. (2015). The Ocean Colour Climate Change Initiative: II. A methodology for assessing atmospheric correction processors based on in-situ measurements. *Remote Sensing of Environment*, 162, 242-256.

Park, Y., and Ruddick, K. (2005). Model of remote-sensing reflectance including bidirectional effects for case 1 and case 2 waters. *Applied Optics* 44:1236–1249.

Patt, F. S., Barnes, R. A., Eplee R. E., Franz, B. A., Robinson, W. D., Feldman, G. C., Bailey, S. W., Gales, J., Werdell, P. J., Wang, M., Frouin, R., Stumpf, R. P., Arnone, R. A., Gould, J. R. W., Martinolich, P. M., Ransibrahmanakul, V., O'Reilly, J. E., and Yoder, J. A. (2003). Algorithm updates for the Fourth SeaWiFS data reprocessing. NASA/TM-2003-206892, Vol. 22, Greenbelt, MD.

Ruddick, K., De Cauwer, V., Park, Y. and Moore, G. (2006). Seaborne measurements of near infrared water-leaving reflectance: The similarity spectrum for turbid waters. *Limnology and Oceanography*, Vol. 51(2) pp. 1167–1179.

Schroeder, T., Behnert, I., Schaale, M., Fischer, J., and Doerffer, R. (2007). Atmospheric correction algorithm for MERIS above case-2 waters. *International Journal of Remote Sensing*, 28, 1469–1486.

Siegel, D. A., M. Wang, S. Maritorena, and W. Robinson (2000). Atmospheric correction of satellite ocean color imagery: The black pixel assumption. *Appl. Opt.* 39(21), 3582–3591.

Spurr, R., K. Stamnes, H. Eide, W. Li, K. Zhang, and J. Stamnes. (2007). Simultaneous retrieval of aerosol and ocean color: A classic inverse modeling approach: I. Analytic Jacobians from the linearized CAO-DISORT model. *J. Quant. Spectrosc. Radiative Transfer*. 104, 428-449.

Steinmetz, F., Deschamps, P.-Y., and Ramon, D. (2011). Atmospheric correction in presence of sun glint: application to MERIS. *Optics Express*, Vol. 19, Issue 10: 9783-9800.

Steinmetz F., Ramon, D., Deschamps, P. Y. (2015). POLYMER atmospheric correction algorithm. ESA OC-CI Algorithm Theoretical Basis Document, Issue 2.0.

Valente, A., Sathyendranath, S., Brotas, V., Groom, S., Grant, M., Taberner, M., Antoine, D., Arnone, R., Balch, W. M., Barker, K., Barlow, R., Bélanger, S., Berthon, J.-F., Besiktepe, S., Brando, V., Canuti, E., Chavez, F., Claustre, H., Crout, R., Frouin, R., García-Soto, C., Gibb, S. W., Gould, R., Hooker, S., Kahru, M., Klein, H., Kratzer, S., Loisel, H., McKee, D., Mitchell, B. G., Moisan, T., Muller-Karger, F., O'Dowd, L., Ondrusek, M., Poulton, A. J., Repecaud, M., Smyth, T., Sosik, H. M., Twardowski, M., Voss, K., Werdell, J., Wernand, M., and Zibordi, G. (2016). A compilation of global bio-optical in situ data for ocean-colour satellite applications, *Earth Syst. Sci. Data*, 8, 235-252.

Wang, M., and Gordon, H.R. (2002). Calibration of ocean color scanners: how much error is acceptable in the near infrared? *Remote Sensing of Environment*, 82: 497-504.

Werdell, P. J. and Bailey, S. W. (2005). An improved in-situ bio-optical data set for ocean color algorithm development and satellite data product validation. *Remote Sens. Environ.* 98, 122–140.

World Meteorological Organization (WMO) (2010). Implementation plan for the global observing system for climate in support of the UNFCCC (2010 update). GCOS report 138.

World Meteorological Organization (WMO) (2011). Systematic observation requirements for satellite-based data products for climate (2011 update). GCOS report 154.

Zibordi, G., Berthon, J.-F., Bulgarelli, B., D'Alimonte, D., van der Linde, D., Mélin, F., and Targa, C. (2004). Ocean color validation activities at the Acqua Alta Oceanographic Tower in the Northern Adriatic Sea. *International Journal of Remote Sensing*, 25, 1533–153.

Zibordi, G., Holben, B., Hooker, S. B., Mélin, F., Berthon, J. -F., Slutsker, I., Giles, I., Vandemark, D., Feng, H., Rutledge, K., Schuster, G., and Al Mandoos, A. (2006a). A network for standardized ocean color validation measurements. *EOS Trans. AGU*, 87(293), 297.

Zibordi, G., Strömbeck, N., Mélin, F., and Berthon, J.-F. (2006b). Tower based radiometric observations at a coastal site in the Baltic Proper. *Estuar. Coast. Shelf Sci.* 69, 649–654.

Zibordi, G., Berthon, J. F., Mélin, F., D'Alimonte, D. and Kaitala, S. (2009a). Validation of satellite ocean color primary products at optically complex coastal sites: Northern Adriatic Sea, northern Baltic Proper and Gulf of Finland. *Remote Sens. Environ.* 113: 2574-2591.

Zibordi, G., Holben, B. N., Slutsker, I., Giles, D., D'Alimonte, D., Mélin, F., Berthon, J.-F., Vandemark, D., Feng, H., Schuster, G., Fabbri, B. E., Kaitala, S., and Seppäl, J. (2009b). AERONET-OC: a network for the validation of ocean color primary radiometric products. *J. Atmos. Ocean. Technol.* 26, 1634–1651.

Zibordi, G., Melin, F., Voss, K., Johnson, B., Franz, B., Kwiatkowska, E., Huot J-P., Wang, M., and Antoine D. (2015). System vicarious calibration for ocean color climate change applications: Requirements for in situ data. *Remote Sensing of Environment*. 159 361-369.

List of Acronyms

Acronym	Description
---------	-------------

ADF	Auxiliary data file
C2RCC	Case 2 Regional Coastcolour Processor
ESA	European Space Agency
MOBY	Marine Optical Buoy
NASA	National Aeronautics and Space Agency
OCB	EUMETSAT Ocean Colour Database
OC-CCI	Climate Change Initiative Ocean Colour
OCR	Ocean Colour Radiometry
OMAPS	Ocean Colour Multi-Mission Algorithm Prototype System
OWT	Optical Water Type
RR-AC	Round Robin Atmospheric Correction, a module of the <i>offline processor</i> subsystem of the Ocean Colour Multi-Mission Algorithm Prototype System
RR-IW	Round Robin In-Water, a module of the <i>offline processor</i> subsystem of the Ocean Colour Multi-Mission Algorithm Prototype System
SeaWiFS	Sea Viewing Wide Field of View Sensor
SRF	Spectral Response Function
SVC	System Vicarious Calibration
TOA	Top of atmosphere
VAL	Validation and Product Assessment module of the <i>offline processor</i> subsystem of the Ocean Colour Multi-Mission Algorithm Prototype System

1 Introduction

1.1 Scope of the document

This ATBD describes the System Vicarious Calibration (SVC) method to be implemented in the Offline Processor within the OMAPS project. SVC is a crucial step in the processing of ocean colour missions to meet the stringent requirements in absolute accuracy and across-sensor consistency of the Ocean Colour Radiometry (OCR), so far unachievable by instrumental calibration alone (Zibordi et al., 2015; Mazeran et al., 2017).

This ATBD deals with the SVC gains computation, to be done in the offline mode once and for all for a given Ocean Colour (OC) processing chain. The gains have then to be applied as a simple correction of the Level-1b radiometry in the operation mode.

The algorithm described hereafter relies on the ESA OC-CCI development (Mazeran et al., 2019). It handles both the standard and alternative OC atmospheric corrections (AC). The ATBD illustrates the method for POLYMER processing chain.

1.2 Context of SVC

The goal of OMAPS is to develop a modular prototype supporting the algorithmic activities of EUMETSAT in Ocean Colour (OC). The fundamental output of OMAPS Level-2 processor is the Ocean Colour Radiometry (water-leaving radiance), which is one Essential Climate Variables (ECV) related to the biological state of the world's ocean (WMO 2010). Water-leaving radiance in the visible spectrum is of utmost concern, since it is the primary data used to derive other ECVs such as chlorophyll-a concentration. It results from correction of the radiometry acquired by the sensor at top of atmosphere (TOA) and can be formally seen as the output of the system comprising sensor and processing chain. OMAPS Product Requirement has retained the very stringent requirements of 5% uncertainty in the blue and green channels, which shall be further narrowed down to 0.5% stability over a decade for potential climate studies (WMO 2011, Zibordi et al. 2015).

Vicarious calibration is the classical approach developed in the OC community to address the required accuracy in OCR. Applied after the instrumental radiometric calibration (i.e. pre-launch as well as post-launch), it consists of adjusting the TOA radiometry through the use of ground-truth measurements, generally high-quality water-leaving reflectance, concurrent with space acquisitions. In practice, a vicarious calibration method produces gains at each validation point and each wavelength that make the sensor + processing chain system exactly match the field measurements.

The concept of vicarious calibration has been introduced very early in ocean colour remote-sensing (e.g. Gordon 1987) in order to meet the specified accuracy of the water-leaving radiance, which forms only a small portion of the radiance measured at the sensor. To understand this aspect, let us restate the classical modelling of the reflectance at sensor level ρ_{TOA} , at a given wavelength λ :

$$\rho_t(\lambda) = t_g(\lambda) \cdot (\rho_R(\lambda) + \rho_a(\lambda) + \rho_{Ra}(\lambda) + t(\lambda)\rho_w(\lambda)) \quad (1)$$

Where t_g is the transmittance for gaseous absorption, ρ_R , ρ_a and ρ_{Ra} are respectively the reflectance for pure Rayleigh scattering, pure aerosol and multiple-scattering between air molecules and aerosols, ρ_w is the desired water-leaving reflectance and t the total upward and downward transmittance of the atmosphere. This formulation ignores implicitly diffuse reflection from whitecaps and sun glint contribution, which can be achieved by avoiding observations at high wind speed and the geometry of specular reflection. In the following we will always deal with reflectance (ρ), instead of radiance (L) primarily measured by the sensor, by using the following conversion:

$$\rho(\lambda) = \frac{\pi L(\lambda)}{F_0(\lambda) \cos \theta_s} \quad (2)$$

Where F_0 is the extraterrestrial solar irradiance at time of acquisition and θ_s the solar zenith angle.

The contribution of the marine signal to ρ_{TOA} is generally around 10% to 15%; over very clear waters the highest contributions occur in the blue wavelengths. Thus, the above-mentioned requirement of 5% accuracy for the water leaving reflectance translates into an accuracy of 0.5% for the TOA reflectance, which is already out of the scope of instrumental calibration (Eplee et al. 2011, Delwart and Bourg 2013). The atmospheric correction (AC) process, whose goal is to retrieve ρ_w from measurement of ρ_{TOA} , adds further uncertainty which can be substantial. Hence vicarious calibration has been historically introduced to complete the imperfect instrumental radiometric calibration, compensate AC errors and reach a higher performance for the whole system.

This general consideration must however be clarified by considering the exact link between ρ_w and ρ_{TOA} . Atmospheric correction consists formally of inverting Eq. (1):

$$\rho_w(\lambda) = \frac{\frac{\rho_t(\lambda)}{t_g(\lambda)} - (\rho_R(\lambda) + \rho_a(\lambda) + \rho_{Ra}(\lambda))}{t(\lambda)} \quad (3)$$

In standard atmospheric corrections (e.g. Gordon and Wang 1994, Antoine and Morel 1999), the unknown aerosol signal, involving atmospheric reflectance and transmittance is inferred from two near-infrared (NIR) bands only. For instance, the SeaWiFS algorithm uses band 765 nm and 865 nm to compute the aerosol optical thickness and to identify the aerosol model. From a spectral point of view, this means that $\rho_w(\lambda)$ depends on the TOA radiometry at band λ itself in the visible and at two other bands in the NIR. If the NIR bands are well-calibrated, then the TOA relative error $\frac{\Delta\rho_t}{\rho_t}$ in the visible leads to a relative error at sea level of:

$$\frac{\Delta\rho_w}{\rho_w}(\lambda) = \frac{\Delta\rho_t}{\rho_t}(\lambda) \left/ \frac{t_g t \rho_w(\lambda)}{\rho_t(\lambda)} \right. \quad (4)$$

The denominator of (4) represents exactly the contribution of marine reflectance to TOA signal. This equation justifies the well-known rule previously stated: “If $t\rho_w$ is 10% of ρ_t , and we want ρ_w with an uncertainty of $\pm 5\%$, one would expect that it would be necessary to know ρ_{TOA} with an uncertainty of no more than $\pm 0.5\%$ ” (Gordon 1998). More recently the basic equation (4) has been exploited in detail by Zibordi et al. (2015) to derive specifications for the quality of in-situ data for the purpose of Climate Data Records (CDRs). However, it is important to emphasise that this overall algebra is intrinsically linked to the standard atmospheric correction scheme, in particular to the decoupling between all bands in the visible as well as to the supposed perfect calibration of NIR bands. This is why the system of sensor and processing chain must be considered as a whole, and has led to the concept of system vicarious calibration, SVC (Gordon 1987, Evans and Gordon 1994). In particular, the first attempts for SeaWiFS tried to simultaneously calibrate both visible and NIR bands (Gordon 1998, Eplee et al. 2001). It is worth noting that Gordon (1998) concluded the previous rule with following statement, which is not important for standard atmospheric correction but very relevant in the present study: “However, as several bands are used in the atmospheric correction of a single band, the variation of the calibration error from band to band is also important”.

1.3 Reminder of the standard method

While several approaches have been tested since end of the 1980s, we will restate only the successful method of Franz et al. (2007) which has been operationally used by NASA for SeaWiFS, MODIS and MERIS, and applied with minor adaptation also by ESA to MERIS (Lerebourg et al. 2011) since third reprocessing. As with any system vicarious calibration, it relies strongly on the atmospheric correction scheme applied (Gordon and Wang 1994, Patt et al. 2003) and in particular on two key aspects:

- A decoupling between NIR and visible bands: two bands in the NIR are used to detect the atmosphere (aerosol content), and the atmospheric correction is successively applied in the visible
- A decoupling between all visible bands: the correction is applied independently band per band

For historical reasons we will refer the class of atmospheric correction algorithms that fulfils these criteria to as *standard atmospheric correction*, in contrast to alternative approaches coupling all bands in the visible and in the NIR. As a consequence, it enables an independent (successive) vicarious calibration of the NIR and visible bands, which we will also refer to as *standard*.

For any wavelength, in both regions of the spectrum, the method seeks to reconstruct the true (or targeted) TOA signal ρ_t^t by the use of indirect measurements or assumptions. Comparison with actual sensor acquisition provides vicarious calibration gains:

$$g(\lambda) = \frac{\rho_t^t(\lambda)}{\rho_t(\lambda)} \quad (5)$$

In essence, vicarious calibration assumes that these gains, computed in ideal conditions, represent a systematic bias of the sensor and processing chain system.

In the NIR, the targeted signal is computed over stable and homogenous oligotrophic waters, where the marine signal can be neglected:

$$\rho_t^t(\lambda_{NIR}) = t_g(\lambda_{NIR})(\rho_R(\lambda_{NIR}) + \rho_a^t(\lambda_{NIR}) + \rho_{Ra}^t(\lambda_{NIR})) \quad (6)$$

The method assumes that the aerosol model is known (maritime atmosphere) and that the longest wavelength is already well calibrated (for example, NASA uses $g(865) = 1$ for SeaWiFS and $g(869) = 1$ for MODIS). It is then possible to predict the TOA signal at the shortest NIR wavelength and deduce a calibration factor. After this NIR calibration, all quantities derived by the atmospheric correction can be considered as reference: aerosol signal $\rho_a^t(\lambda) + \rho_{Ra}^t(\lambda)$ and diffuse transmittance $t^t(\lambda)$, at any wavelength λ .

In the visible, the targeted signal is computed through the use of reference in-situ marine reflectance $\rho_w^t(\lambda)$, acquired concurrently with the satellite measurement:

$$\rho_t^t(\lambda) = t_g(\lambda)(\rho_R(\lambda) + \rho_a^t(\lambda) + \rho_{Ra}^t(\lambda) + t^t(\lambda)\rho_w^t(\lambda)) \quad (7)$$

The criticality of these in-situ measurements, which calibrate ocean colour mission at global scale and on the long-term, requires rigorous protocols in the instrumentation as well as in the match-up with satellite data (Mueller et al. 2003, Bailey and Werdell 2006).

We insist on the fact that the targeted signal in Eq. (7) is constructed with very same elements as that of the atmospheric correction, cf. Eq. (3), in particular radiative transfer look-up tables, so that there is a perfect consistency between atmospheric correction and calibration. By construction, the system vicarious calibration in the visible will make the algorithm exactly match the in-situ signal, whatever the real source of error in the system (from sensor or algorithm or probably from both).

Technically, vicarious gains given in Eq. (5) are first computed pixel by pixel for each match-up. The perfect match with in-situ data demonstrates the relevance of these so-called individual gains. The pixel-per-pixel gains are then spatially averaged, providing a unique gain per match-up, for each wavelength. Eventually, matchup-per-matchup gains are temporally averaged, yielding a unique set of gains $\bar{g}(\lambda)$ at each wavelength, over the entire mission lifetime. In order to minimise impact of outliers, Franz et al. (2007) have used the mean

of the semi-interquartile range (MSIQR, mean of data within the 25th and 75th percentiles) for both spatial and temporal averaging:

$$\bar{g}(\lambda) = \underset{time}{\text{MSIQR}} \left(\underset{space}{\text{MSIQR}}(g(\lambda)) \right) \quad (8)$$

Because of the variability in marine reflectance errors, the mean gains \bar{g} in the visible can only remove biases, i.e. average systematic errors. Hence the reference dataset must be representative of most common atmospheric and marine conditions.

1.4 Challenge of SVC for non-standard AC

In the last decade there has been an emergence of alternative ocean colour algorithms which do not use the NIR to identify aerosol and may even not follow the standard formulation (Eq. (3)). These atmospheric correction makes use of most of the available radiometry from blue to NIR channels, with the objective of better addressing optically complex waters with significant scattering in the NIR, of being more robust to radiometric noise, of having a larger spectral basis for better aerosol propagation or of inverting more complex physical effects such as thin clouds, sun glint residual and absorbing aerosols. Without being comprehensive, most of these techniques refer to as either artificial neural networks (e.g. Doerffer and Schiller 2007, Schroeder et al. 2007), spectral matching algorithms (e.g. Chomko et al. 2003, Spurr et al. 2007, Kuchinke et al. 2009, Steinmetz et al. 2011) or more recently a Bayesian approach (e.g. Frouin and Pelletier 2015). Within the OC-CCI project, POLYMER (Steinmetz et al. 2011) is a candidate algorithm for building the CDRs, has been successfully tested in a first phase on the MERIS sensor (Müller et al. 2015) and is under consideration for harmonisation with the SeaWiFS and MODIS-Aqua datasets. It is described in more detail in the next section and will serve as a practical case to illustrate our findings.

A common feature of all these approaches is to determine either explicitly or implicitly the atmospheric path signal from knowledge of several bands in the visible, and possibly the NIR bands, what requires embedding a marine model in the algorithm. This is as opposed to the standard approach, based on the black pixel assumption in the NIR, which does not, at least for clear waters, impose any modelling hypothesis on the marine reflectance (Gordon 1978, Siegel et al. 2000). From a purely radiometric point of view, the retrieval of marine reflectance at band λ_i by any atmospheric correction scheme can be formally written by:

$$\rho_{wN}(\lambda_i) = f_i(\rho_t(\lambda_1), \dots, \rho_t(\lambda_n)), \quad i = 1 \dots m \quad (9)$$

where the m functions f_i express the link to TOA radiometry and may also depend on other non-radiometric parameters such as ancillary data, geometrical conditions, physical constants, etc., not made explicit in the present context. These functions may be more or less complex depending on the atmospheric correction scheme, and may even not be explicit, such as in artificial neural networks. In Eq. (9) we note n the number of TOA bands used as input to the atmospheric correction and m the number of bottom of atmosphere (BOA) bands at which a marine reflectance is provided, with $m \leq n$. Note also that for convenience we deal with fully normalised water-leaving reflectance ρ_{wN} (see Morel and Gentili 1996 for Case-1 waters), that is we include the bidirectional reflectance distribution function (BRDF) correction in functions f_i for a direct comparison with in-situ measurements in normalised condition.

Such algorithms make the standard SVC approach inoperative for two reasons. The first technical reason is that Eq. (9) is not algebraically invertible (assuming that it would even be invertible), making it impossible to reconstruct the targeted TOA signal ρ_t^t from knowledge of the target marine signal ρ_{wN}^t . Hence the definition of vicarious calibration gains Eqs. (5)-(7) simply cannot be applied. The second reason is that the SVC approach relies intrinsically on the linear response of the marine reflectance in one band with respect to the TOA signal at this very same band (see Eq. (3)). This decoupling and linearity are no longer true with non-standard

atmospheric corrections, so that changing (calibrating) the radiometry at one band also impacts the marine reflectance at other bands. This effect is illustrated in Figure 1 for a typical MODIS TOA spectrum over clear water, processed on the one hand by the SeaDAS standard algorithm (Baith et al 2001) and on the other hand by POLYMER (Steinmetz et al. 2011, see detailed description in section 2.2.3). In both cases the remote-sensing marine signal, prior to any SVC, is too high when compared to the in-situ measurement at all bands and especially by around 25% at 412 nm. A calibration gain of -1% is then applied on $\rho_t(412)$ and results into:

- A relative change of about -7% on $\rho_w(412)$ only, in case of SeaDAS
- A relative change of less than -2% on ρ_w at 412 nm, becoming positive and growing with wavelength, from about +3% at 443 nm to +30% at 667 nm, in case of POLYMER

This example shows that it may be possible to make the POLYMER $\rho_w(412)$ match the in-situ measurement by decreasing $\rho_t(412)$, but with a much greater amplitude than for SeaDAS. More importantly, this change causes biases in other bands and calibrating the TOA signal at other bands also impacts $\rho_w(412)$. Hence the vicarious gain at 412 nm cannot be computed independently.

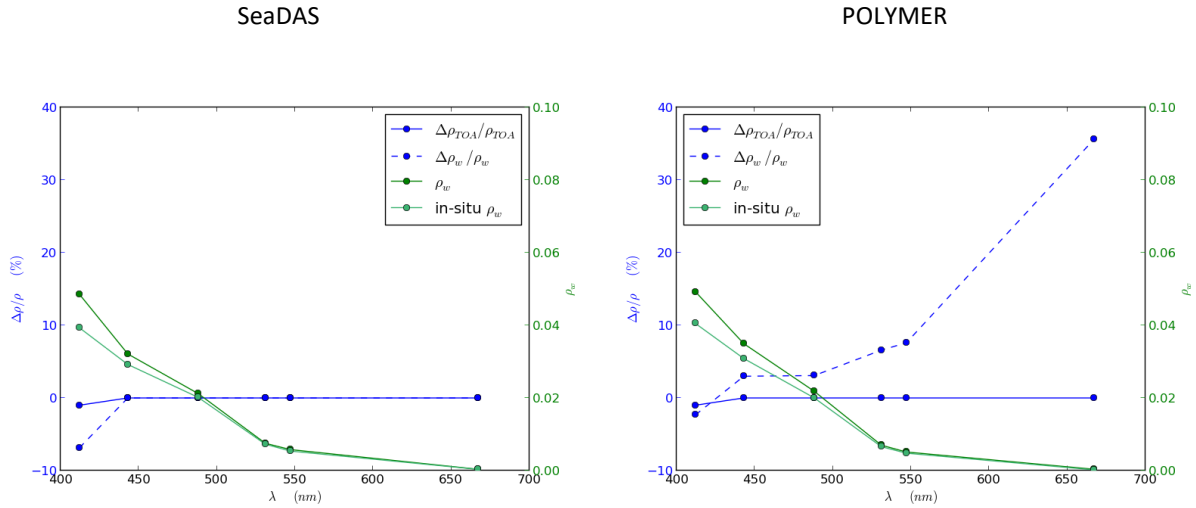


Figure 1. Relative change of the marine reflectance (dashed blue) due to a TOA relative change of 1% at 412 nm (solid blue, left Y-axis), for SeaDAS algorithm (left) and POLYMER (right) over a typical clear water spectrum. Clear and dark green lines represent respectively the in situ and satellite marine reflectance (right Y-axis)

1.5 Generalising the SVC definition

Since atmospheric correction schemes following the generic formalism of Eq. (9) preclude computing the gains with standard equations (5)-(7), we propose generalising the definition of gains. The intrinsic definition of a set of SVC gains (g_1, g_2, \dots, g_m) associated to wavelengths $\lambda_1, \lambda_2, \dots, \lambda_m$ is that it allows the exact retrieval of the targeted signal ρ_{wN}^t at the same bands; this can be written as

$$f_i(g_1 * \rho_t(\lambda_1), \dots, g_m * \rho_t(\lambda_m), \rho_t(\lambda_{m+1}), \dots, \rho_t(\lambda_n)) = \rho_{wN}^t(\lambda_i), \quad i = 1 \dots m \quad (10)$$

In its most generic form, Eq. (10) must be understood as a non-linear system of m equations and m unknowns, which defines implicitly the gains. It is important that the number of gains cannot be greater than the number of available information, m , so that $n - m$ bands cannot be vicariously calibrated. For the sake of simplicity, we have sorted the m calibrated channels in the lowest positions, without any assumption on the real order of the wavelengths.

We will refer to Eq. (10) as the *strict* SVC problem because a strict retrieval of the in-situ data is expected, in accordance with the standard SVC definition. This definition however does not ensure existence and

uniqueness of a solution, which is the general impediment of any non-linear system, depending on the non-linearity of the atmospheric correction (i.e. of functions f_i). It is demonstrated in Mazeran et al. (2019) that the strict SVC problem applied to POLYMER allows solution only under very particular conditions, and furthermore that there is a multiplicity of possible gains. The only way to deal with such cases is to solve Eq. (10) in a weaker sense, i.e. in a least-square sense. For such purpose we will define the *optimal* SVC problem as finding a set of l gains $g = (g_1, g_2, \dots, g_l)$ with $l \leq m \leq n$ which minimises the discrepancy between the retrieved and targeted marine signal, for a given χ^2 cost function:

$$\chi_{SVC}^2(g) = \sum_{i=1}^m \left(\rho_{wN}^t(\lambda_i) - f_i(g_1 * \rho_t(\lambda_1), \dots, g_l * \rho_t(\lambda_l), \rho_t(\lambda_{l+1}), \dots, \rho_t(\lambda_n)) \right)^2 \quad (11)$$

This minimisation problem also provides an implicit definition of the gains, but now ensures existence of at least one solution to the SVC. Furthermore, if by chance the strict SVC admits a solution, then it will also be a solution of the optimal SVC. Hence this latter formalism will be considered by default in the following. Note that the cost function χ_{SVC}^2 could be refined by weighting each square of the sum, typically by uncertainty at each band, without changing the aim of this paper. This option is not retained in the present work, first because of lack of knowledge in the remote-sensing uncertainty and second because of spectrally white uncertainty of the MOBY data considered here (between 2 and 4% from 412 to 666nm, see Brown et al. 2007).

A noticeable difference between the strict (Eq. (10)) and optimal (Eq. (11)) SVC is the number of bands to be calibrated. The strict SVC needs as many TOA gains as marine reflectance bands, i.e. m . On the contrary the optimal SVC can relax the number of gains to $l \leq m$, although all m information at BOA are kept in the cost function. For example, we may search gains at two bands (λ_1, λ_2) to best match in-situ data of four bands $(\lambda_1, \lambda_2, \lambda_3, \lambda_4)$, keeping in mind that the TOA radiometry at the two first bands impacts all four bands at BOA. This flexibility will be used to solve the issue of non-uniqueness.

Finally let us emphasise that this revisited definition of SVC in Eq. (11) is a natural extension of the standard SVC formalism (Eqs. (5)-(7)), in the sense that it leads to the same gains when applied to the standard atmospheric correction scheme. This can be verified by fitting the standard scheme Eq. (3) in our general formalism with

$$f_i(\rho_t(\lambda_1), \dots) = C_{BRDF}(\lambda_i) \frac{\frac{\rho_t(\lambda_i)}{t_g(\lambda_i)} - (\rho_R(\lambda_i) + \rho_a(\lambda_i) + \rho_{Ra}(\lambda_i))}{t(\lambda_i)}, \quad i = 1 \dots m \quad (12)$$

Where $C_{BRDF}(\lambda_i)$ is the BRDF correction factor converting marine reflectance from sensor geometry (ρ_w) to normalised geometry (ρ_{wN}). This factor generally depends on the bio-optical content just beneath the sea surface, which in operation can only be deduced from the radiometry and induces a spectral coupling in the ρ_{wN} . In the context of vicarious calibration, this knowledge is provided by the in-situ data, breaking the dependence of C_{BRDF} on the sensor radiometry. Remember also that atmospheric quantities do not depend on radiometry of bands 1 ... m . Thus f_i are simple linear functions of $\rho_{TOA}(\lambda_i)$ only and the optimal SVC problem, computable through $\nabla \chi_{SVC}^2 = 0$, simplifies immediately to the strict SVC problem, written as a linear system:

$$J \begin{pmatrix} \rho_t(\lambda_1) & \dots & 0 \\ \vdots & \ddots & \vdots \\ 0 & \dots & \rho_t(\lambda_m) \end{pmatrix} \begin{pmatrix} g_1 \\ \vdots \\ g_m \end{pmatrix} - \begin{pmatrix} \tilde{\rho}_{path}(\lambda_1) \\ \vdots \\ \tilde{\rho}_{path}(\lambda_m) \end{pmatrix} = \begin{pmatrix} \rho_{wN}^t(\lambda_1) \\ \vdots \\ \rho_{wN}^t(\lambda_m) \end{pmatrix} \quad (13)$$

Where $\tilde{\rho}_{path}(\lambda_i) = C_{BRDF}(\lambda_i)(\rho_R(\lambda_i) + \rho_a(\lambda_i) + \rho_{Ra}(\lambda_i)) / t(\lambda_i)$ and the Jacobian matrix J of the atmospheric correction is diagonal:

$$J = \begin{pmatrix} \frac{C_{BRDF}(\lambda_1)}{t_g(\lambda_1)t(\lambda_1)} & \dots & 0 \\ \vdots & \ddots & \vdots \\ 0 & \dots & \frac{C_{BRDF}(\lambda_m)}{t_g(\lambda_m)t(\lambda_m)} \end{pmatrix} \quad (14)$$

The trivial solution is given by:

$$g_i = \frac{t_g(\lambda_i) \left(\rho_R(\lambda_i) + \rho_a(\lambda_i) + \rho_{Ra}(\lambda_i) + t(\lambda_i) \frac{\rho_{WN}^t(\lambda_i)}{C_{BRDF}(\lambda_i)} \right)}{\rho_t(\lambda_i)}, \quad i = 1 \dots m \quad (15)$$

We recognise identical gains as the standard definition in Eqs. (5)-(7), with $\frac{\rho_{WN}^t}{C_{BRDF}}$ being the targeted marine signal converted to sensor geometry.

2 Algorithm description

2.1 Processing outline

SVC gains are computed in two steps: first computation of individual gains per match-ups, then temporal averaging. The first step is the main and more time-consuming task, and can be considered as the core of the SVC module. To achieve it, the module needs as input (Figure 2):

- A database of match-ups between in-situ data and Level-1b satellite data (see sections 2.2.1 and 2.2.2);
- Actual Level-1b products covering the database;
- The Level-2 OC processor (see section 2.2.3), comprising notably the ADF which contains the SVC gains.

In order to be generic and applicable to any optical sensor and processor, the module considers the Level-2 processor as a black box. For a given match-up, the black box is launched iteratively to compute the SVC gains (see section 2.3) through a so-called Level-2 wrapper. The role of the wrapper is to launch through a unique generic command line any Level-2 processor, for any Level-1 product, ADF and region of interest, and then convert the Level-2 product in the standardised match-up database format. The Level-2 wrapper has to be created for any Level-2 processor (see section 2.6) and is thus a complementary input of the SVC module, in parallel of the Level-2 processor itself. The ADF is updated at each iteration, and at convergence provides the final SVC gain for the considered match-up.

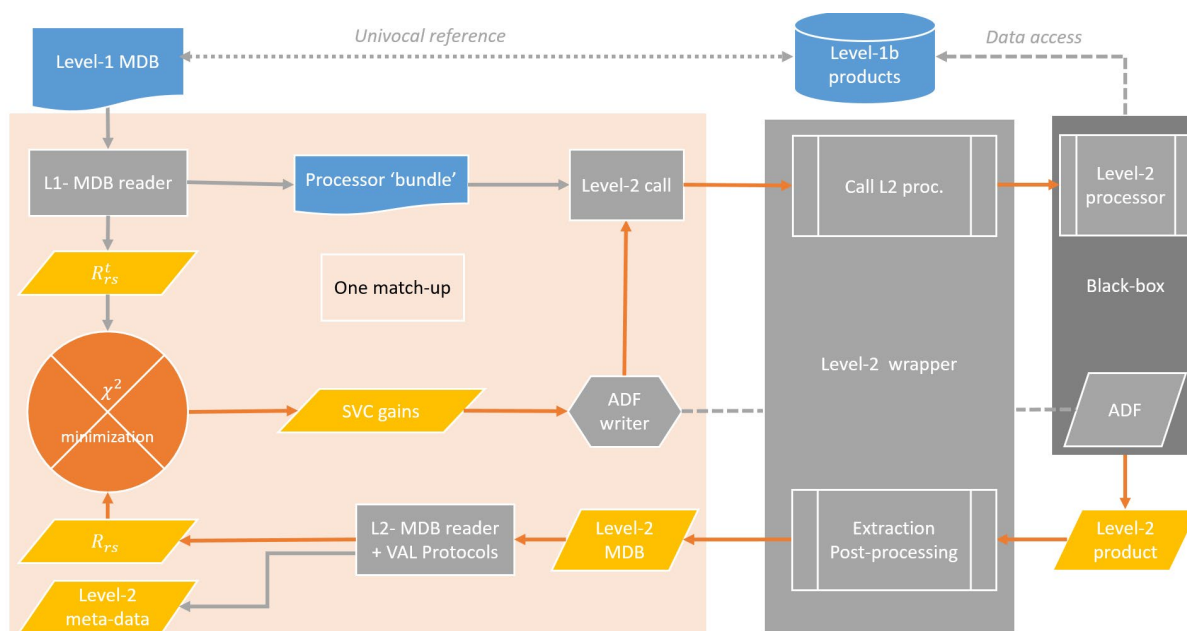


Figure 2 Processing outline of the SVC computation.

2.2 Algorithm input

2.2.1 In situ data

The single source of in-situ data considered for present vicarious calibration is the Marine Optical BuoY (MOBY), located off the Lanai Hawaiian island (Clark et al. 2003). This is a natural choice since these measurements are used by all agencies for the operational SVC of OC sensors. Furthermore, and independent of its high quality and appropriateness for vicarious calibration (e.g. Zibordi et al. 2015), the MOBY dataset has the rare advantage of exhibiting systematically measurements at all visible bands of all sensors, which is strictly required in the present context of spectrally coupled atmospheric correction.

The MOBY dataset used for the present SVC comes directly from the EUMETSAT OC-SVC-TOOL study. It notably accounts for the integration of MOBY hyperspectral measurements over the OLCI-A and OLCI-B spectral response functions, and selects the most relevant depth propagation. For full details on this dataset we refer the reader to the EUMETSAT report of Mazeran and Ruescas (2020), section 4.1.2.

2.2.2 EO data and match-ups

Match-ups between the reference data and the satellite data are in theory generated by the OMAPS match-up module. Here we have simply started from the existing Match-up Database (MDB) at EUMETSAT, already used in the OC-SVC-TOOL study for the calibration of the OLCI operational processor (Mazeran and Ruescas, 2020). Hence, direct comparison of the SVC gains between the OMAPS and operational processors is achievable.

2.2.3 OC processor

SVC can be applied indifferently to all OC processors considered in the OMAPS online mode. We summarise below the case of POLYMER, which has justified the development of the non-standard SVC method in the OC-CCI project.

POLYMER atmospheric correction was first introduced in Steinmetz et al. (2011) for the MERIS sensor and stands for "POLYNomial based algorithm applied to MERIS". Its initial motivation was to correct for the sun glint effect, which affects a large part of the MERIS swath. Authors showed a roughly equivalent performance of the inversion inside and outside the glint area, hence increasing the usual coverage of MERIS data. The algorithm has since been updated within the ESA OC-CCI project as described in Steinmetz et al. (2015). The

main difference consists in using an alternate water reflectance model including bidirectional correction to sun at zenith and sensor at nadir, based on Park and Ruddick (2005) and more suited to case 2 waters than the previous model. Other updates relate to of numerical inversion, atmospheric parameterization and the adaptation to other sensors. Both water reflectance parameterisations were tested and it is worth noting that, while they obviously impact the marine reflectance and the exact vicarious calibration gains, they do not change our overall conclusion.

In POLYMER, a preliminary sun glint reflectance is estimated from the Cox and Munk (1954) model relating sea surface roughness to wind speed and acquisition geometry. This contribution is tabulated simultaneously with Rayleigh scattering (including coupling between both) and contains potentially large errors due to only approximate knowledge of the wind field at pixel scale. The core of the atmospheric correction is then built upon an ocean-atmosphere radiometric model, in which coupled inversion over the full spectrum seeks to retrieve the residual sun glint, together with aerosol signal and any other atmospheric contributor (e.g. undetected thin cloud). This atmospheric and glint residual component, noted ρ_{ag} , is modelled by a function of λ consisting of three terms:

$$\rho_{ag}(\lambda, c_0, c_1, c_2) = c_0 T_0(\lambda) \lambda^{p_0} + c_1 \lambda^{p_1} + c_2 \rho_R(\lambda) \quad (16)$$

We refer to Steinmetz et al. (2015) for a detailed description of this modelling, where the exponents $p_0 = 0$, $p_1 = -1$ and third term in $\rho_R(\lambda)$ are chosen to represent spectrally flat components (attenuated by a mixed direct/diffuse transmittance $T_0(\lambda)$), aerosol, and coupling with Rayleigh respectively. Coefficients (c_0, c_1, c_2) are the atmospheric unknowns. The marine model, noted ρ_w^{mod} , is inevitably required when atmospheric correction deals with wavelengths in the visible (see e.g. Bricaud and Morel (1987) for a precursor approach on CZCS). The earliest version of POLYMER relies on the Morel and Maritorena (2001) model parameterised by chlorophyll concentration, modified to also take into account backscattering of non-covarying particles and extended beyond 700 nm by the similarity spectrum of Ruddick et al. (2006). Some bio-optical constraints have been further added in Steinmetz et al. (2015), so that we shall simply keep the generic notation $\rho_w^{mod}(\lambda, \varphi)$ where φ represents a set of biological unknowns. The present analysis does not need a more explicit form, except to count the degrees of freedom, here two. In the end POLYMER relies on following TOA formulation:

$$\rho_t(\lambda) = t_g(\lambda) \left(\rho_R(\lambda) + \rho_{ag}(\lambda, c_0, c_1, c_2) \right) + t(\lambda) \left(\rho_w^{mod}(\lambda, \varphi) + \varepsilon(\lambda) \right) \quad (17)$$

Where $\varepsilon(\lambda)$ is the BOA residual resulting from inherent discrepancy between the full model and the TOA radiometry. Note that ρ_R is here a shorthand which implicitly contains the Cox and Munk sun glint (term $\rho_{mot+gli}$ in Steinmetz et al. 2011). Moreover, the diffuse transmittance $t(\lambda)$ includes only the Rayleigh part and it is thus known from auxiliary data. The actual TOA quantity involved in POLYMER optimisation is the radiometry corrected for gaseous absorption, Rayleigh and sun glint, noted ρ_{Rc} hereafter:

$$\rho_{Rc}(\lambda) = \frac{\rho_t(\lambda)}{t_g(\lambda)} - \rho_R(\lambda) \quad (18)$$

It follows that given a set of atmospheric and bio-optical parameters $(\hat{c}_0, \hat{c}_1, \hat{c}_2, \hat{\varphi})$, both terms ρ_{ag} and ρ_w^{mod} can be evaluated and marine reflectance is retrieved at any wavelength by:

$$\rho_w(\lambda) = \frac{\rho_{Rc}(\lambda) - \rho_{ag}(\lambda)}{t(\lambda)} = \rho_w^{mod}(\lambda, \hat{\varphi}) + \varepsilon(\lambda) \quad (19)$$

Importantly the second equality shows that this reflectance is also the sum of ρ_w^{mod} and the residual $\varepsilon(\lambda)$ (by definition of Eq. 17), so that POLYMER final product is not strictly speaking the output of a marine model. The left part of Eq. (19) differs essentially from standard atmospheric correction (Eq. (3)) in the way the ρ_{ag} term is computed. POLYMER first reduces the dimensionality of the non-linear problem by linking the atmospheric

unknowns to the bio-optical unknowns. Indeed, for any ρ_w^{mod} , the coefficients can be best evaluated by minimising a linear least-square problem:

$$\left\{ \begin{array}{l} (\hat{c}_0, \hat{c}_1, \hat{c}_2) = \underset{(c_0, c_1, c_2)}{argmin} \chi_{atm}^2 \\ with \chi_{atm}^2 = \sum_{i=1}^n (T_0(\lambda_i) c_0 \lambda_i^{p_0} + c_1 \lambda_i^{p_1} + c_2 \rho_R(\lambda_i) - (\rho_{Rc}(\lambda) - t(\lambda_i) \rho_w^{mod}(\lambda_i, \varphi)))^2 \end{array} \right. \quad (20)$$

These coefficients are thus a linear combination of $\rho_w^{mod}(\lambda_i, \varphi)$ and provide, through ρ_{ag} , a marine reflectance depending on φ , noted $\rho_w(\lambda, \varphi)$. Then POLYMER minimises the discrepancy between this retrieved reflectance and the marine model, with respect to the φ unknown only:

$$\hat{\varphi} = \underset{\varphi}{argmin} \chi_{bio}^2(\varphi) \quad where \quad \chi_{bio}^2(\varphi) = \sum_{i=1}^n \left(\frac{\rho_w(\lambda, \varphi) - \rho_w^{mod}(\lambda_i, \varphi)}{\sqrt{\rho_w^{mod}(\lambda_i, \varphi)}} \right)^2 \quad (21)$$

Numerator of Eq. 21 is exactly the residual $\varepsilon(\lambda)$. Root square in denominator weights the cost function according to the amplitude of the marine signal at different wavelengths (with a threshold of 0.005, not made explicit here). The spectral coupling over the full spectrum appears clearly in minimisation of cost functions χ_{atm}^2 and χ_{bio}^2 , built upon all available n bands of the sensor.

2.3 Theoretical description

2.3.1 Data screening

For vicarious gain computation and pixel-by-pixel verification at MOBY, we follow as much as possible protocols of the standard SVC defined in Franz et al. (2007): time difference between satellite and ground measurement less than three hours, sun zenith angle less than 70°, view zenith angle less than 56°, chlorophyll concentration at MOBY lower than 0.2 mg/m³, 5x5 macro-pixel extractions around the in-situ point without any flagged pixel. Due to its robustness, POLYMER is quite permissive in the data screening and provides few quality flags. Hence only pixels flagged by POLYMER as cloud or with an explicit atmospheric correction failure are discarded (negative particulate backscattering, out of bound parameters in the minimisation). After careful consideration, pixels impacted by sun glint have been kept as valid because of POLYMER's capability to well perform under such condition and also because such data are considered in the Level-2 OC-CCI dataset.

2.3.2 Sensitivity of AC

Vicarious gains for non-standard atmospheric correction are all spectrally coupled. A relevant object to inspect the spectral coupling of the SVC problem is the Jacobian matrix of the generic function f defining the atmospheric correction in Eq. (9):

$$\nabla f = \begin{pmatrix} \frac{\partial f_1}{\partial x_1} & \dots & \frac{\partial f_1}{\partial x_n} \\ \vdots & \ddots & \vdots \\ \frac{\partial f_m}{\partial x_1} & \dots & \frac{\partial f_m}{\partial x_n} \end{pmatrix} \quad (22)$$

This matrix expresses the sensitivity of the BOA quantity (marine reflectance) on the TOA radiometry; its coefficients can be written more explicitly by $\partial f_i / \partial x_j = \partial \rho_{wN}(\lambda_i) / \partial \rho_t(\lambda_j)$. An example of such matrix is given on Figure 3, for a typical clear water pixel and at six wavelengths in the visible ($m = n = 6$). Note that its computation requires numerical differentiation, as will be described in next section. The colour of each cell represents the absolute value of the partial derivative, while the sign is written in the cell. In the SeaDAS example (left image), the NIR iteration scheme (Bailey et al. 2010) has been de-activated, which yields a

diagonal matrix: thus, the decoupling of the standard atmospheric correction. Looking into details actually shows a slight extra-diagonal dependence in $\rho_t(443)$ and $\rho_t(547)$, due to the bidirectional effect correction, using these two bands in the chlorophyll estimate (Morel and Gentili 1996); this sensitivity is, however, extremely small compared to the diagonal terms. The right image displays the Jacobian matrix over same condition for POLYMER and shows a totally different structure. First the matrix is no longer diagonal, characteristic of the spectral coupling. Then for a given row (i.e. given $\partial\rho_{wN}(\lambda_i)$), diagonal terms are sometimes smaller than extra-diagonal terms: which means that the spectral constraints of the atmospheric correction are stronger than the TOA radiometry itself. For instance, $\rho_{wN}(412)$ is much more sensitive to $\rho_t(488)$ and $\rho_t(531)$ than to $\rho_t(412)$ itself. Also relative change between bands may be of opposite sign: for instance a positive change at $\rho_t(443)$ increases $\rho_{wN}(531)$ but a positive change at $\rho_t(531)$ decreases $\rho_{wN}(443)$. Eventually, bands near the red, such as 547 and 667nm, are weakly sensitive to the TOA radiometry (rows $\partial\rho_{wN}(547)$ and $\partial\rho_{wN}(667)$), but inversely they impact marine reflectance in the blue (columns $\partial\rho_t(547)$ and $\partial\rho_t(667)$), so are part of the SVC problem.

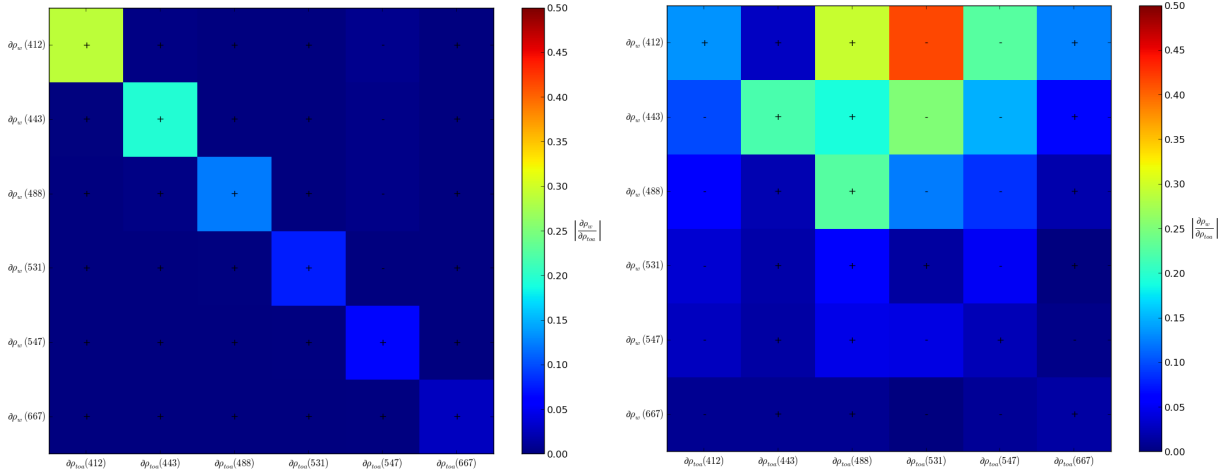


Figure 3. Jacobian matrix on a typical clear water pixel for SeaDAS (left) and POLYMER (right).

Hence, the structure of the Jacobian matrix illustrates the complexity of the vicarious calibration problem, which is now described as a problem of BOA sensitivity to the TOA radiometry. In this respect the behaviour of algorithms such as POLYMER is significantly different compared to standard atmospheric corrections. The sensitivity shall guide the choice of bands to be used in the gain computation.

2.3.3 SVC in the VIS

We first introduce vector and matrix notation to deal more easily with the spectral dimension. Unless explicitly mentioned, the dimension is n (number of bands used in the atmospheric correction) and we note:

$$\rho = \begin{pmatrix} \rho(\lambda_1) \\ \vdots \\ \rho(\lambda_n) \end{pmatrix} \quad (23)$$

For the sake of readability, we start by studying the optimisation problem of Eq. (11) in the simple case $l = m = n$, and will deal with the general case just after. Let us call F the function relating vicarious gains to the retrieved marine reflectance:

$$\begin{aligned} F: \mathbb{R}^n &\rightarrow \mathbb{R}^n \\ g &\rightarrow F(g) = \begin{pmatrix} f_1(g_1 * \rho_t(\lambda_1), \dots, g_n * \rho_t(\lambda_n)) \\ \vdots \end{pmatrix} \end{aligned} \quad (24)$$

This is just another writing of functions f_i , directly expressed with respect to gains instead of TOA radiometry. In particular, we have $F(1) = \rho_{wN}$, i.e. the marine reflectance without any vicarious calibration. The cost function then simply writes $\chi_{SVC}^2(g) = \|\rho_{wN}^t - F(g)\|^2$ and its minimum is solution of the $n \times n$ non-linear system

$$\nabla F'(\rho_{wN}^t - F(g)) = 0 \quad (25)$$

Where ∇F is the Jacobian matrix of F , evaluated at current g , and the prime superscript stands for its transpose. There is an obvious link between ∇F and the Jacobian matrix J of function f previously defined in Eq. (22); notably for $g = 1$ we have:

$$\nabla F(1) = \begin{pmatrix} \rho_t(\lambda_1) \frac{\partial \rho_{wN}(\lambda_1)}{\partial \rho_t(\lambda_1)} & \cdots & \rho_t(\lambda_n) \frac{\partial \rho_{wN}(\lambda_1)}{\partial \rho_t(\lambda_n)} \\ \vdots & \ddots & \vdots \\ \rho_t(\lambda_1) \frac{\partial \rho_{wN}(\lambda_n)}{\partial \rho_t(\lambda_1)} & \cdots & \rho_t(\lambda_n) \frac{\partial \rho_{wN}(\lambda_n)}{\partial \rho_t(\lambda_n)} \end{pmatrix} \quad (26)$$

Such system can only be solved numerically, especially if the atmospheric correction of concern is not explicit. Any standard computational method can be candidate, albeit it requires iterative runs of the atmospheric correction, on a pixel-per-pixel basis. The OC-SVC-TOOL makes flexible the number of iterations:

- A unique iteration (one-step inversion) is the default option, based on the fact that calibration gains are expected to be small with respect to unity, typically less than 5%, and with limited non-linearities. Any larger value would originate from a major problem in either the instrumental calibration or the atmospheric correction itself, and would need a dedicated correction beyond the scope of vicarious calibration.
- More iterations are possible to solve for non-linearities.

For a given iteration, a first order Taylor expansion around $g = g_0$ writes $F(g) \approx F(g_0) + \nabla F(g_0)(g - g_0)$ and allows Eq. (25) to be solved approximately with the $n \times n$ linear system:

$$\nabla F' \nabla F(g - g_0) = \nabla F'(\rho_{wN}^t - \rho_{wN}) \quad (27)$$

Here ∇F is implicitly defined at $g = g_0$ and ρ_{wN} is computed for the gain g_0 (by default or previous iteration). This solution can be interpreted as one iteration of the Gauss-Newton algorithm minimising χ_{SVC}^2 . Now, when dealing with the general case of gains retrieval for l bands only, with a cost function defined on m bands with $l \leq m \leq n$, the very same algebra is true when considering in Eq. (27) the $m \times l$ submatrix of ∇F and restricting $\rho_{wN}^t - \rho_{wN}$ to m rows. Due to multiplication with matrix $\nabla F'$, Eq. (27) is then simply a $l \times l$ linear system.

Note that if the strict SVC were possible, with an equal number of unknowns and equations ($l = m$), Eq. (27) would be equivalent to the linear system $\nabla F(g - g_0) = \rho_{wN}^t - \rho_{wN}$, which now would be interpreted as one iteration of the Newton-Raphson algorithm to solve the strict problem $F(g) = \rho_{wN}^t$. It follows that our solution is exact for a linear atmospheric correction (with respect to the TOA radiometry); it is indeed an easy exercise to check that it retrieves exactly the standard gains when applied to the standard atmospheric correction, cf. Eqs. (13)-(14)-(15). In this respect we can see the solution of Eq. (27) as a natural generalisation of the standard gain computation Eqs. (5)-(7). Furthermore, the linear system highlights, at first order, the spectral coupling between gains through the Jacobian matrix.

For an algorithm such as POLYMER, when the aerosol component is not analytically given, partial derivatives must be approximated numerically. We use a second order approximation, to have more accuracy in the Jacobian matrix than in the inverse method itself:

$$\frac{\partial f_i}{\partial x_j} \approx \frac{f_i(x_1, \dots, x_j + h_j, \dots, x_n) - f_i(x_1, \dots, x_j - h_j, \dots, x_n)}{2h_j} \quad \text{with } h_j \ll 1 \quad (28)$$

In practice for each calibration scene, these terms are computed by applying POLYMER on $2 * l$ Level1 modified scenes whose TOA signal are $\rho_t(\lambda_j) \pm h_j$ for $j = 1 \dots l$. Note again that this approximate scheme gives exactly the expected vicarious gains for a linear atmospheric correction decoupling all bands. The choice of step h_j depends on how quickly f_i varies with respect to x_j . Numerical tests have convinced us to consider a relative step instead of an absolute step, i.e. $h_j = s * \rho_t(\lambda_j)$. Another advantage is that because of the $\rho_t(\lambda_i)$ factor in Eq. (26), a relative step allows to use either TOA radiance and reflectance as the input variable:

$$L_t \frac{\partial \rho_w(L_t)}{\partial L_t} = \rho_t \frac{\partial \rho_w(\rho_t)}{\partial \rho_t} \quad (29)$$

While we have here described the formalism in term of ρ_t , in practice radiance L_t is used, as it is provided in the Level 1 products. Several trials for various relative steps (from 0.05% to 5%) show that $s = 0.5\%$ or 1% gives a good approximation of the derivative at every wavelength. This is illustrated on Figure 4 for $\frac{\partial \rho_w(443)}{\partial \rho_t(560)}$: the 0.5% differentiation has the closest numerical derivative to the exact derivative computed by spline interpolation. It is noteworthy that increments that are too small yield to totally erroneous values because then numerical differences reach the limit of numerical accuracy and become meaningless.

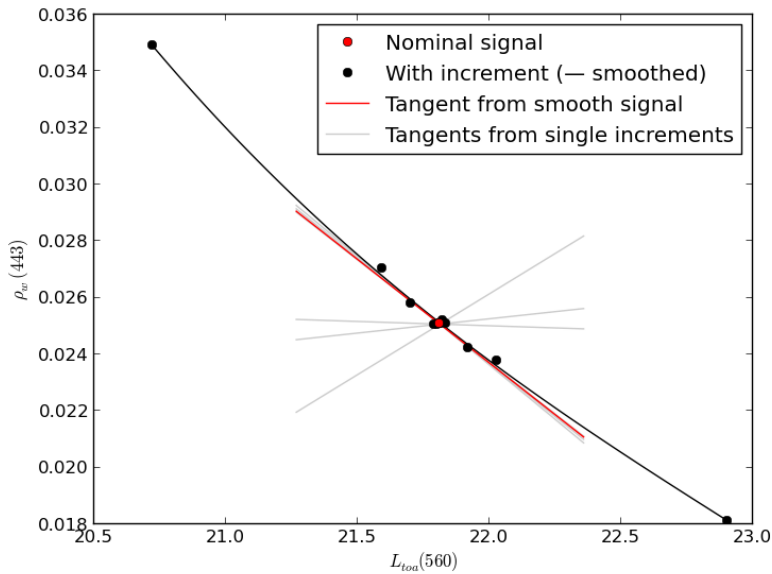


Figure 4. Example of numerical differentiation of $\rho_w(443)$ by $L_t(560)$. The red dot corresponds to nominal signal and ten black dots for modified $L_t(560)$ with step $\pm 5\%$, $\pm 1\%$, $\pm 0.5\%$, $\pm 0.1\%$ and $\pm 0.05\%$ (ordered on the x-axis). Numerical derivative for each step is represented by the tangent lines in grey. The true derivative is computed by spline interpolation and represented by the tangent red line.

To sum up, our numerical method defined by Eqs. (27)-(28) is based on the sole approximation of a first order expansion. Validity of this reduction is directly linked to the degree of linearity of the atmospheric correction with respect to radiometry. Practically, suitability of the computed individual gains will be checked a posteriori, on pixel-by-pixel calibrated data.

2.3.4 SVC in the NIR

For spectrally coupled AC, the NIR and VIS bands have the same role, so that the gain computation described previously in the VIS shall be applied to the whole spectrum without distinction between VIS and NIR; this shall be achieved by a calibration site where in situ marine reflectance in the NIR are either measured or demonstrated to be negligible and set to zero.

For standard AC, SVC in the NIR shall be achieved before SVC in the VIS. Indeed, once the radiometry in the NIR has been calibrated, the aerosol detection (in the NIR) and correction (in the VIS) is independent of the TOA radiometry in the VIS, so that gains in the VIS can be computed consecutively as described before. Individual gains in the NIR are computed through the generic formalism already presented, i.e. minimization of χ_{SVC}^2 . The computation is only a special case with following configuration:

- The database of match-ups is replaced by a database of extractions over oligotrophic waters, namely over the South Pacific Gyre (SPG), where the reference marine reflectance in the NIR is considered as negligible ($\rho_{wN}^t=0$ in the NIR).
- One band in the NIR is fixed (typically 865 nm for OLCI) and not part of the minimization. Gains are computed at all other NIR bands.

The standard AC of the Level-2 processor is constrained by fixing the aerosol selection to the maritime model with 90% relative humidity. This is achieved by creating a dedicated ADF with this unique model instead of the full family of aerosol models.

2.3.5 Mission average gain

Due to the spectral coupling, individual gains for a certain match-up point are only meaningful when defined spectrally. In order to keep this spectral consistency in the mean gains (first per match-up and then per mission), we thus apply the MSIQR of Eq. (8) simultaneously for all calibrated bands. In other words, the spatial (respectively temporal) mean is computed on the same pixels (respectively same match-ups) for all wavelengths. This generally results in a more severe screening than the band-per-band MSIQR: if some gain spectra differ too much from the mean shape, the mean may be based on less than 50% of the initial data.

2.4 Algorithm output

The primary output of the SVC offline module is a set of spectral gains, at all bands of the sensor, stored in the relevant ADF of the Level-2 OC processor. The gains of bands not used in the AC or not selected for SVC by the user are set to unity. Together with the ADF, the SVC module produces complementary outputs to support the analysis of gains:

- Statistics of the individual gains: number, mean, standard deviation, chi-square test (text file);
- Time-series of individual gains and plots versus camera detectors, viewing angle and metadata stored in the match-up database (e.g. meteo data);

Following the requirement {Req-SVC-015}, the SVC module can optionally simulate the TOA signal at the calibration site, consistently with the SVC gains. For a given match-up, this amounts to multiplying the actual radiometry (without SVC) by the associated individual SVC gains. This optional output is a Level-1 match-up database file, similar to the input MDB file with a new field for the TOA radiometry after SVC (e.g. *satellite_OaXX_radiance_SVC* for OLCI band XX).

Last, another set of optional outputs is generated in test mode, when the user wants to check in more details the individual gains. Basically, this corresponds to a set of spectral gains for each match-up, and validation plots to check the effect of per-pixel SVC (see section 2.5 about performance estimate).

2.5 Performance estimates

A major concern of the optimal SVC is to understand how much pixel-by-pixel gains make sense. Because the problem has to be solved numerically, the only way to prove relevance of the individual gains is to apply them at TOA and verify, a posteriori, that they improve retrieval of marine reflectance. This sanity check is mandatory for any SVC implementation, yet in the present situation we cannot expect a perfect match with the in-situ data. Such an exercise is illustrated on Figure 5 in the POLYMER/OLCI-A case (see section 2.7 for more details on the SVC configuration). Comparison between in-situ and satellite data is clearly improved after pixel-by-pixel calibration, although the retrieval is not perfect, contrary to what would be achieved with a standard AC. The disappointing results at 560 nm (still presenting a significant improvement) is likely due to the necessary trade-off between bands in the optimal SVC, and more precisely because present χ_{SVC}^2 cost function is expressed in absolute value; this penalises band at 560 nm whose marine reflectance is respectively four and seven times smaller than that at 490 and 412 nm. For all bands, a limit is also due to the marine model embedded in the AC (comprising also BRDF correction), which might not be able to perfectly match the in situ data at MOBY, as explained below.

The initially large dispersion between ρ_{wN} and ρ_{wN}^t at pixel level, visible on left panel of Figure 5, explains through Eq. (27) why all individual gains are also scattered (see Figure 6 in section 2.7.2), although some statistical post-processing allows computing more robust average value. This has obvious implication on the relevance of mean vicarious gains when SVC is run in operation: too much scattering means that SVC will not significantly improve performance at match-up level. This is why SVC is classically understood in a statistical sense, to remove bias on average. However, even on average, the optimal SVC differs from the standard case. Indeed, for standard atmospheric correction and standard SVC, applying a mean gain \bar{g} yields a new signal $\rho_w^{\bar{cal}}$ satisfying:

$$\rho_w^{\bar{cal}}(\lambda) - \rho_w^t(\lambda) = (\bar{g}(\lambda) - g(\lambda)) \frac{\rho_t(\lambda)}{t_g(\lambda)t(\lambda)} \quad (30)$$

Averaging this relation over all calibration points demonstrates the perfect bias removal at each band, whatever the scattering in the gains (note that for a strict bias removal, averaging of g should be weighted by the TOA signal propagated at BOA, contrary to the usual practice). Non-linearity in POLYMER prevents to write such relationships. To make this point more explicit, let us consider general vector notations:

$$\begin{aligned} \rho_w^{\bar{cal}} - \rho_w^t &= F(\bar{g}) - \rho_w^t \\ &= F(\bar{g}) - F(g) + (F(g) - \rho_w^t) \\ &\approx \nabla F(g)(\bar{g} - g) + (\rho_w^{cal} - \rho_w^t) \end{aligned} \quad (31)$$

We remind that ∇F is a $m \times l$ matrix, with m being the number of bands considered at BOA and l the number of bands vicariously calibrated at TOA. The first term of right-hand side of Eq. (31) expresses the difference in ρ_w between mean and individual calibration and is the counterpart of Eq. (30) for a generic coupled atmospheric correction. The second term expresses the error due to the individual gain and would therefore vanish for standard atmospheric correction. For POLYMER we have seen that this term is not zero, and furthermore that ∇F is not invertible (even in the case where $m = l$), so that it is impossible to define a mean gain \bar{g} which would remove exactly the bias. In fact, the best mean gain should satisfy another optimisation problem, now over the full time-series of match-ups, which is not of interest in the present study. Our point in Eq. (31) is to show that, even with a hypothetical set of individual gains weakly scattered around their mean \bar{g} , the bias does remain because of the $\rho_w^{cal} - \rho_w^t$ contribution, inherently linked to the imperfection of the marine model.

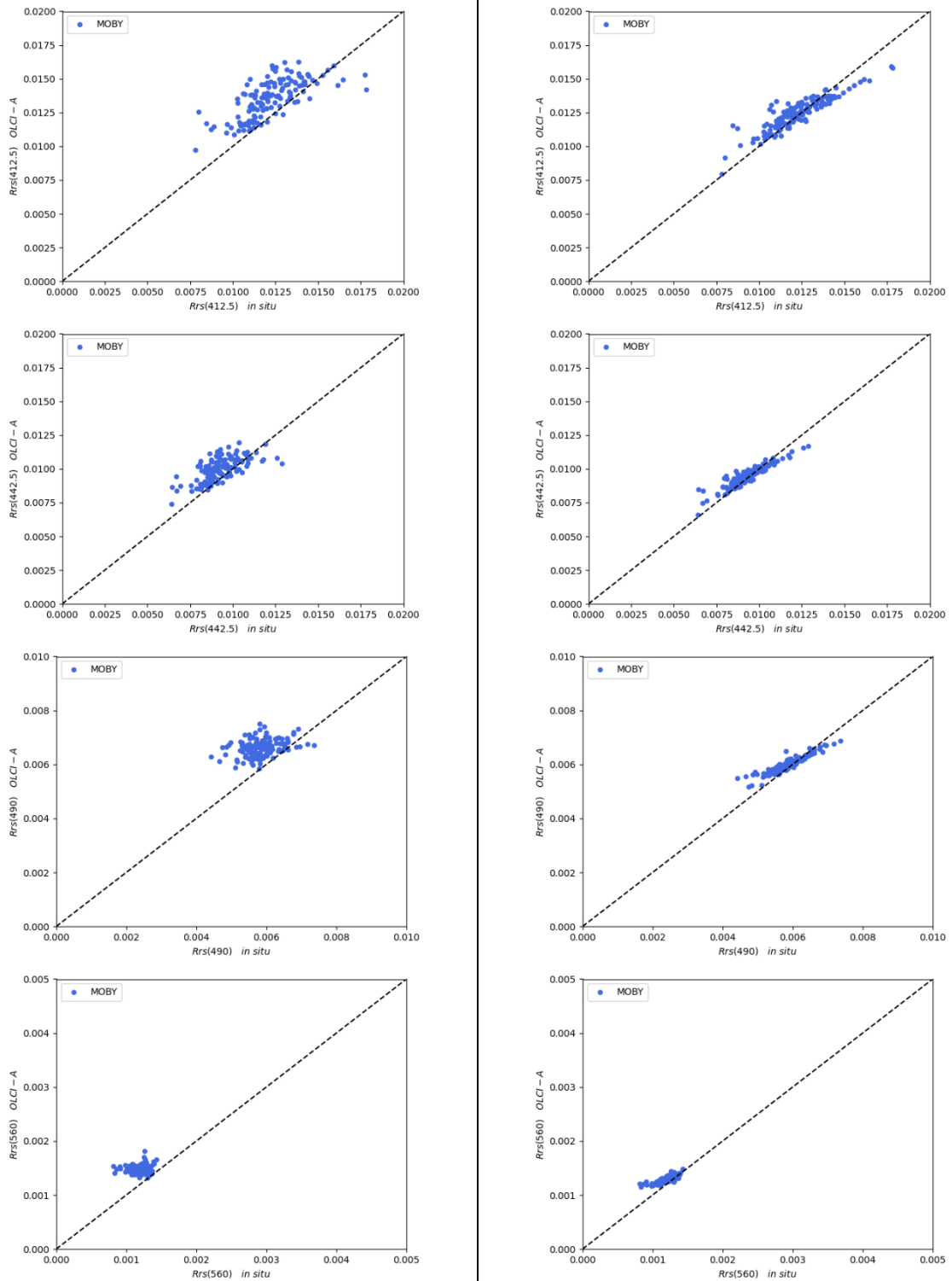


Figure 5. Validation of OLCI-A Rrs at MOBY before (left) and after (right) applying pixel-by-pixel gains.

2.6 Practical considerations

The offline SVC module has been developed for EUMETSAT as a stand-alone software, called OC-SVC-TOOL. The source code of the software, developed in Python, can be downloaded from EUMETSAT Gitlab server <http://gitlab.eumetsat.int>, project OC/External/OC-SVC-TOOL. The software runs on Linux environment and requires Python 3. It is operated through a Graphical User Interface (GUI) giving access to two main functionalities: first the computation of individual SVC gains over a given match-ups database; second the post-processing and analysis of these individual gains, up to the provision of mission average gains which shall be applied in operation. The software is developed for being generic, i.e. multi-mission, multi-processor. The functionalities of the OC-SVC-TOOL software fulfil all OMAPS requirements for SVC, and are more largely compliant with protocols and requirements inherited from the OC community and EUMETSAT own practices. This covers the data selection, data screening and post-processing, proposed with default options to the user in the GUI.

The Level-2 wrapper has to be created by the user for any Level-2 processor. The calling sequence must follow this convention:

```
wrapper_executable --ADF ADF_file --PDU PDU_file --lat lat_IS --lon lon_IS  
--MP size --outdir output_dir [options]
```

where:

- `ADF_file` is the auxiliary data file containing the SVC gains; other ADFs required by the Level-2 processor shall be handled directly in the wrapper itself;
- `PDU_file` is the Level-1 PDU to be processed;
- `lat_IS` and `lon_IS` are the latitude and longitude of the calibration site;
- `size` is the size of the macro-pixel, in pixel, around the central pixel closest to the in situ measurement (size=5 means a 5x5 macro-pixel);
- `output_dir` is the output directory where the Level-2 product will be created.
- `options` are a list of optional parameters to be given to the Level-2 processor for user' specific purpose, outside the SW-TOOL specifications.

More detailed practical considerations about the installation and use of the software are available in the OC-SVC-TOOL documentation (DOC-TOOL, EUMETSAT deliverable ref. EUM/19/SVCT/D2).

2.7 Results

2.7.1 Case studies and configurations

The validation is here conducted for two sensors, OLCI-A and OLCI-B, and two processors available in OMAPS:

- The SACSO processor, version 1, contractually delivered by HYGEOS to EUMETSAT in July 2021 and available at <https://gitlab.eumetsat.int/Chimot/sacso>. The SACSO code is actually able to run in various configurations; in the following SACSO refers to the default configuration validated during the SACSO study, so-called *params_multifit_nlinear levenberg*.
- POLYMER processor, version 4.13. To ease the interfaces in the context of a single instrument (OLCI), we have used the capability to launch POLYMER from the SACSO code, with the dedicated configuration called *base*. This configuration is similar to the POLYMER version 4.13 developed by HYGEOS.

The SVC problem for spectral matching is complex and gain computation may be unstable. The SACSO code, for both SACSO and POLYMER configurations, allows applying the SVC gains only in the standard sense, i.e. on

the TOA radiometry without impacting the aerosol retrieval (function *run_atm_corr_svc* with option *calib_svc*). This means ρ_w is computed by:

$$\rho_w(\mathbf{g}, \mathbf{g}_0, \lambda) = \frac{\rho_{RC}(\mathbf{g}, \lambda) - \rho_{ag}(\mathbf{g}_0, \lambda)}{t(\lambda)} \quad (32)$$

Where $\rho_{RC}(\mathbf{g}, \lambda)$ is the precorrected signal with application of \mathbf{g} at TOA, and ρ_{ag} is computed after application of a default gains \mathbf{g}_0 defined with the standard option *calib* (but is not impacted by \mathbf{g}). This option is used here during the computation of the SACSO and POLYMER gains, with \mathbf{g} computed iteratively (through the *calib_svc* option) and \mathbf{g}_0 fixed at a given iteration with the value of previous iteration (through *calib* option).

During the gains post-processing, one parameter is of special importance for non-standard AC: the maximum difference between in situ and satellite Rrs, after the individual SVC. For standard AC, the SVC is expected to make the Level-2 processor exactly match the in situ data, but this is impossible for in the present case. If the difference is higher than the threshold at any band where gains have been computed (not full spectrum), the match-up is discarded. Here we set this parameter to 1.E-3.

The calibration is achieved at the MOBY site, with the MDB described in section 2.2. Because we deal with spectral matching algorithm over the whole spectrum, this MDB has been extended in the NIR bands, by setting the in situ marine reflectance to zero (from 709 to 1020 nm).

2.7.2 POLYMER/OLCI-A

The aerosol correction of POLYMER for OLCI data is based on nine bands among the twenty-one available: 443, 490, 510, 560, 620, 665, 754, 779, and 865 nm; seven other bands are not used in the aerosol correction but are still part of the SVC process since marine reflectance are provided: 400, 412, 674, 681, 709, 885 and 1020 nm. As justified by the theoretical analysis, we discard three bands: we select the three last bands, 754, 779, and 865 nm, by fixing their gains to unity. The SVC computations at the thirteen other bands is limited to only one iteration, as done in the OC-CCI.

Individual and averaged spectral gains are plotted on Figure 6, and time-series of individual gains across the mission lifetime is shown on Figure 7. Detailed values and statistics are given in Table 1. Gains in the VIS and at 1020 nm are consistent in term of shape with that of the OLCI-A operational processor (see Mazeran and Ruescas, 2020), although slightly closer to unity, suggesting that part of the SVC adjust for a sensor bias (about 1%) but also that POLYMER is more robust to absolute calibration issue. Noticeable differences are observed at 709 and 885 nm, with a peak far from the overall -1% adjustment of other bands; it is likely due to the water vapour gaseous absorption, not corrected at all in POLYMER. This finding suggests to add a dedicated gaseous correction at these bands in a future POLYMER processor.

The individual gains are robust along time, especially after the MSIQR temporal filtering (dark filled circles in Figure 7), as quantified by low standard-deviation of less than 0.4% and low Relative Standard Error of the Mean (RSEM, see Zibordi et al., 2015) of less than the targeted 0.05% in the VIS.

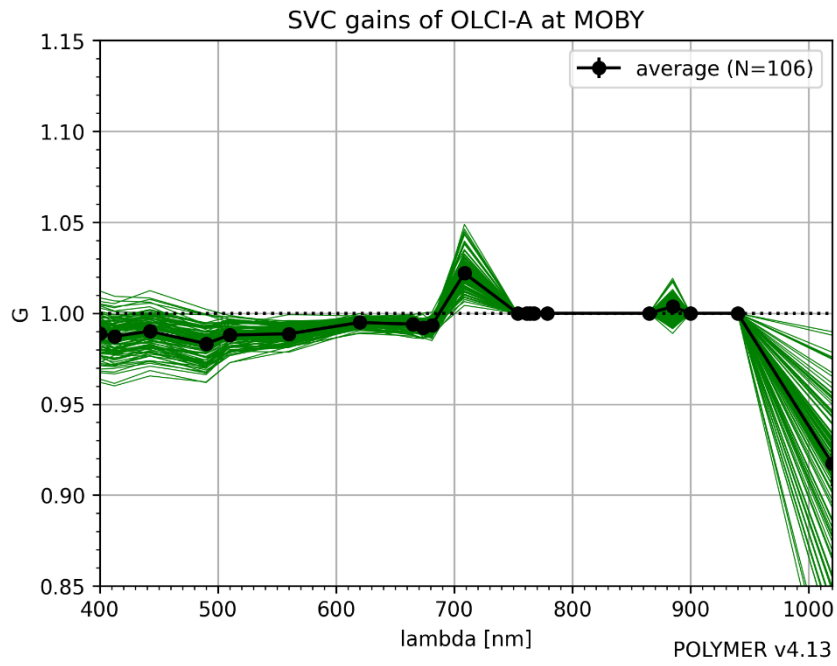


Figure 6. POLYMER vicarious gains derived for OLCI-A at MOBY as a function of wavelength. Solid lines represent individual gains, with dark overlay when they are within the MSIQR. Black line with dots is the constant mission mean gain.

Table 1 Statistics of POLYMER/OLCI-A averaged gains at MOBY, after MSIQR filtering

Wavelength	Number	Average gain	Standard-deviation	RSEM [%]
400	52	0.988766	0.003754	0.0315
412.5	52	0.98731	0.004028	0.0338
442.5	52	0.990117	0.003665	0.0307
490	52	0.983254	0.003184	0.0268
510	52	0.988012	0.002098	0.0176
560	52	0.98867	0.001589	0.0133
620	52	0.994923	0.000768	0.0064
665	52	0.993979	0.000924	0.0077
673.75	52	0.991983	0.001239	0.0104
681.25	52	0.993475	0.001024	0.0085
708.75	52	1.022051	0.003461	0.0281
753.75	106	1	0	0
778.75	106	1	0	0
865	106	1	0	0
885	52	1.003618	0.002238	0.0185
1020	52	0.917483	0.012397	0.112

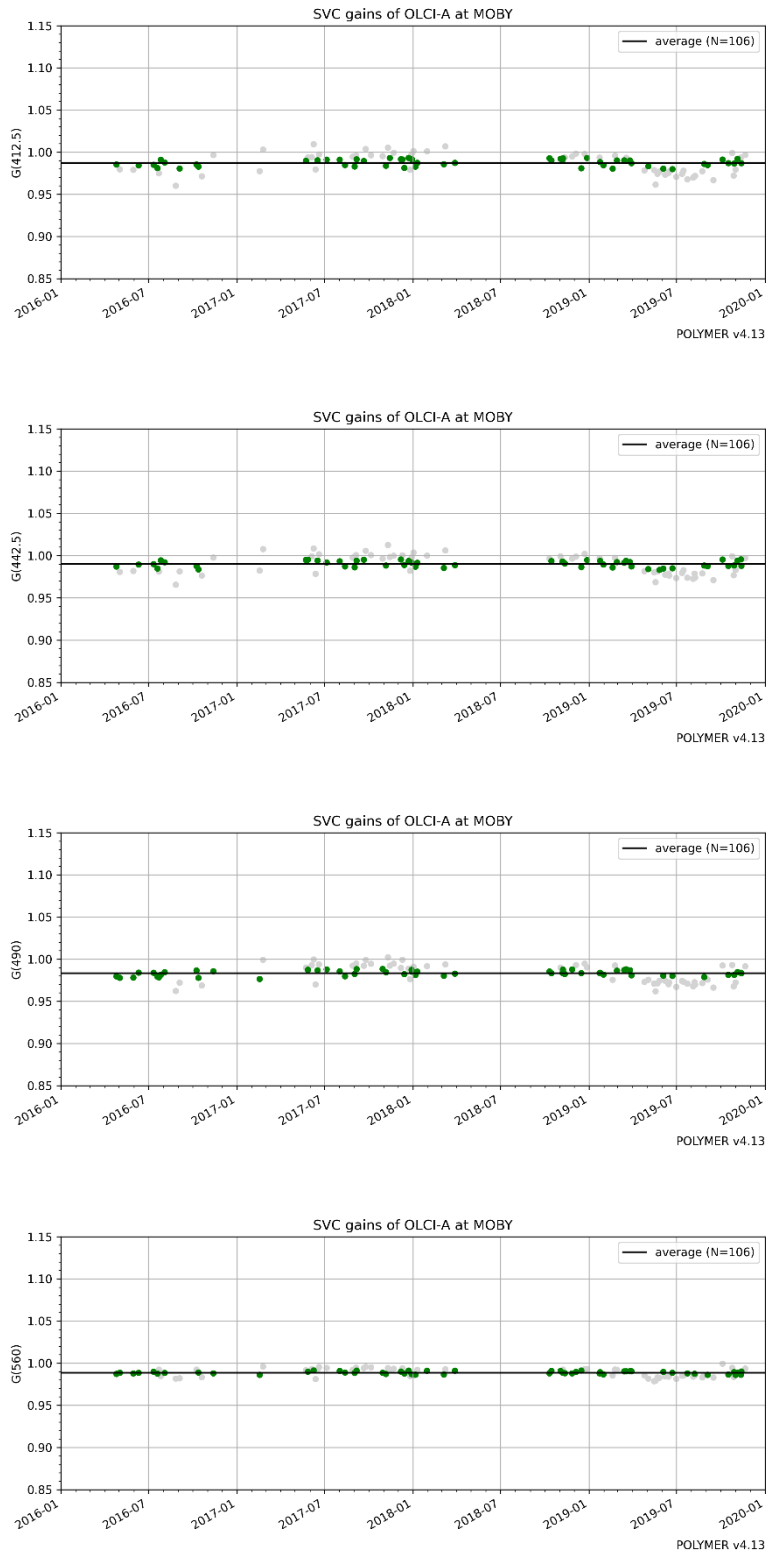


Figure 7. Time-series of POLYMER vicarious gains derived for OLCI-A at MOBY at 412, 443, 490 and 560 (from top to bottom). Circles represent all individual gains, with dark fill when they are within the MSIQR. Black line is the mission average gain.

2.7.3 POLYMER/OLCI-B

The same process is applied to POLYMER/OLCI-B. Similarly to what is observed for the operational OLCI processor, OLCI-B gains for POLYMER are closer to unity than OLCI-A, and with overall similar spectral shape. The dispersion and RSME are once again very low.

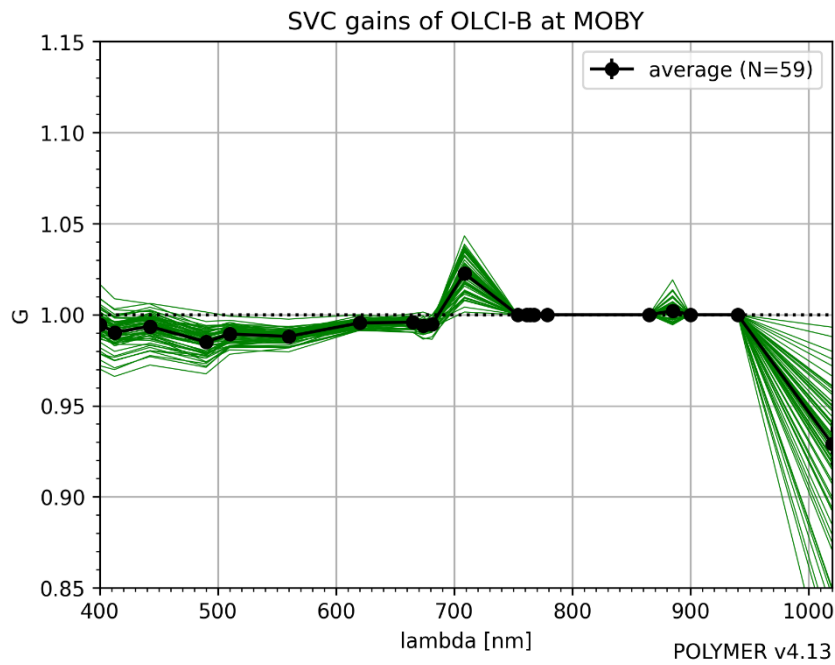


Figure 8. POLYMER vicarious gains derived for OLCI-B at MOBY as a function of wavelength. Solid lines represent individual gains, with dark overlay when they are within the MSIQR. Black line with dots is the constant mission mean gain.

Table 2 Statistics of POLYMER/OLCI-B averaged gains at MOBY, after MSIQR filtering

Wavelength	Number	Average gain	Standard-deviation	RSEM [%]
400	29	0.994505	0.003154	0.0196
412.5	29	0.99026	0.003189	0.0199
442.5	29	0.993551	0.003029	0.0188
490	29	0.985061	0.002669	0.0167
510	29	0.989383	0.001923	0.012
560	29	0.988082	0.000985	0.0062
620	29	0.995495	0.000718	0.0045
665	29	0.995889	0.000982	0.0061
673.75	29	0.993886	0.001107	0.0069
681.25	29	0.994687	0.001031	0.0064
708.75	29	1.022696	0.003167	0.0191
753.75	59	1	0	0
778.75	59	1	0	0
865	59	1	0	0
885	29	1.002101	0.001854	0.0114
1020	29	0.928988	0.012335	0.0819

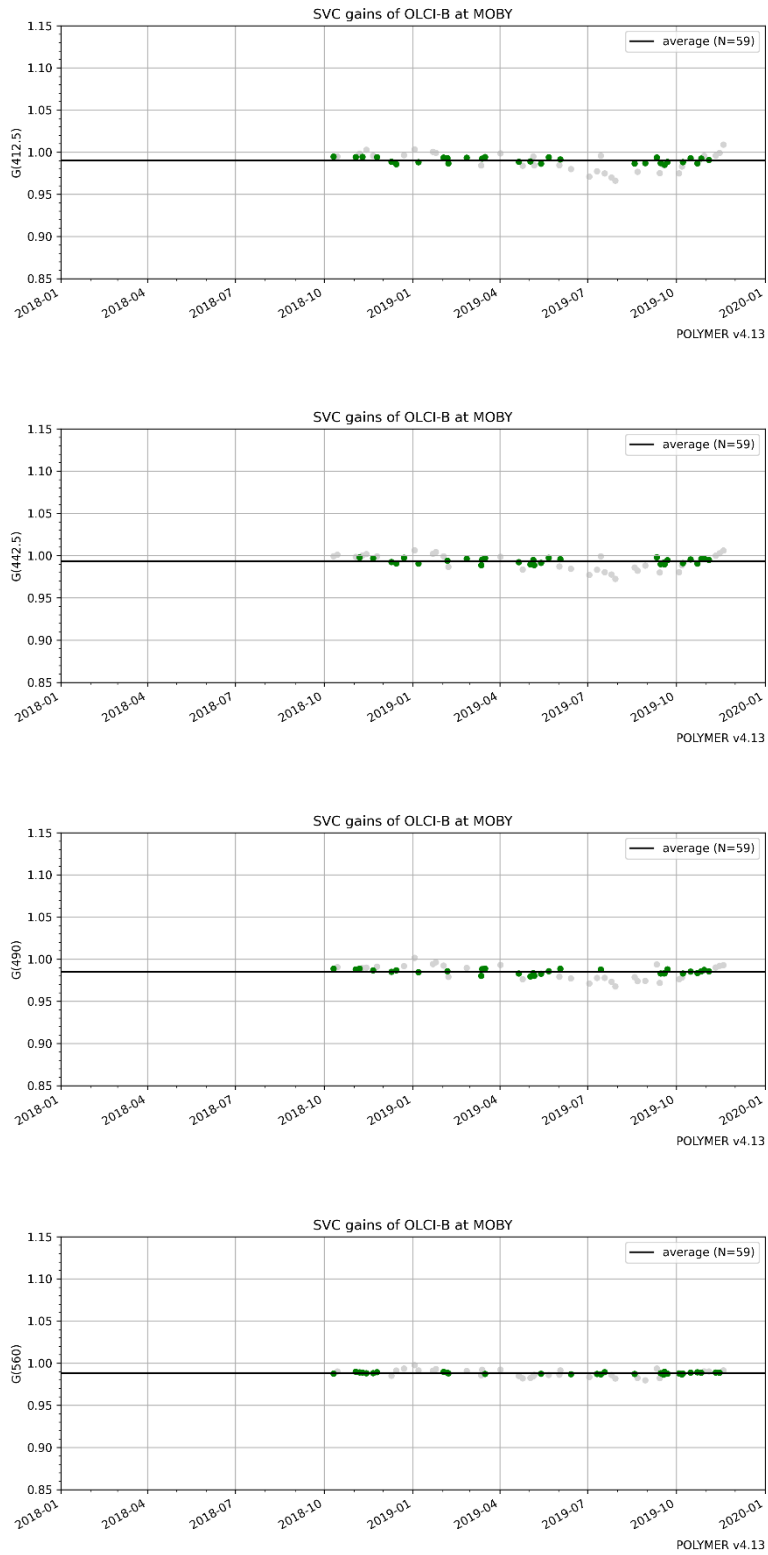


Figure 9. Time-series of POLYMER vicarious gains derived for OLCI-B at MOBY at 412, 443, 490 and 560 (from top to bottom). Circles represent all individual gains, with dark fill when they are within the MSIQR. Black line is the mission average gain.

2.7.4 SACSO/OLCI-A

SVC configuration for SACSO is slightly different than for POLYMER, because the problem of multiplicity of gains that was due to linearity in POLYMER atmospheric model here vanishes. Hence, we can calibrate the sixteen OLCI bands at once, most of them being actually used in the aerosol detection. We have also observed an increase stability in the iterative gain computation, and have allowed 5 iterations per match-up.

Resulting gains, plotted on Figure 10 and given in Table 3, are of about 0.98% in the VIS bands and appears to be extremely close to that of the OLCI standard processor. It could be that, due to its nonlinear and constrained atmospheric model, SACSO cannot solve calibration bias through the atmospheric part (or less than POLYMER), similarly to the standard AC, hence is more sensitive to the instrumental calibration. In the NIR, we recognise the same pattern at 709 and 885 nm as that of POLYMER, since both processors share the same precorrection (i.e. lack of water vapour correction).

SACSO gains are more scattered than that of POLYMER, still with RSEM values close to the target of 0.05% in the VIS. Obviously the choice of 1.E-3 in the maximum difference between in situ and satellite Rrs has an impact on this dispersion. We have checked that taking a smaller threshold would reduce the number of points and the dispersion, but not significantly the average gains, which are quite robust thanks to the MSIQR filtering.

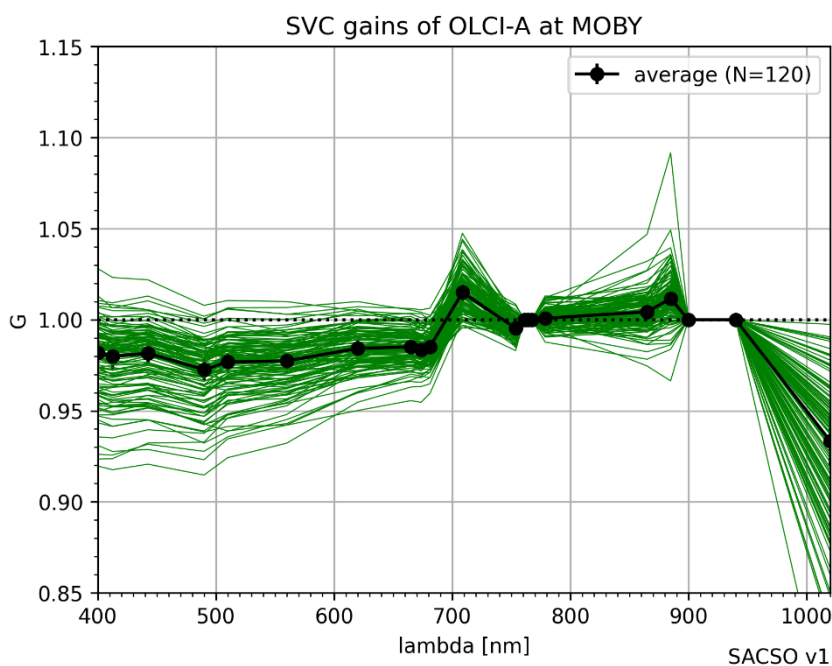


Figure 10. SACSO vicarious gains derived for OLCI-A at MOBY as a function of wavelength. Solid lines represent individual gains, with dark overlay when they are within the MSIQR. Black line with dots is the constant mission mean gain.

Table 3 Statistics of SACSO/OLCI-A averaged gains at MOBY, after MSIQR filtering

Wavelength	Number	Average gain	Standard-deviation	RSEM [%]
400	60	0.98181	0.006752	0.053
412.5	60	0.979885	0.006661	0.0524
442.5	60	0.981551	0.00615	0.0483
490	60	0.972591	0.005712	0.0453
510	60	0.976808	0.00512	0.0404
560	60	0.977369	0.004526	0.0357
620	60	0.98424	0.004259	0.0334
665	60	0.985055	0.003552	0.0278
673.75	60	0.983324	0.003301	0.0259
681.25	60	0.985154	0.003474	0.0272
708.75	60	1.014972	0.004844	0.0368
753.75	60	0.995357	0.002107	0.0163
778.75	60	1.00077	0.00185	0.0143
865	60	1.004331	0.003383	0.026
885	60	1.011602	0.003591	0.0274
1020	60	0.933486	0.014174	0.1171

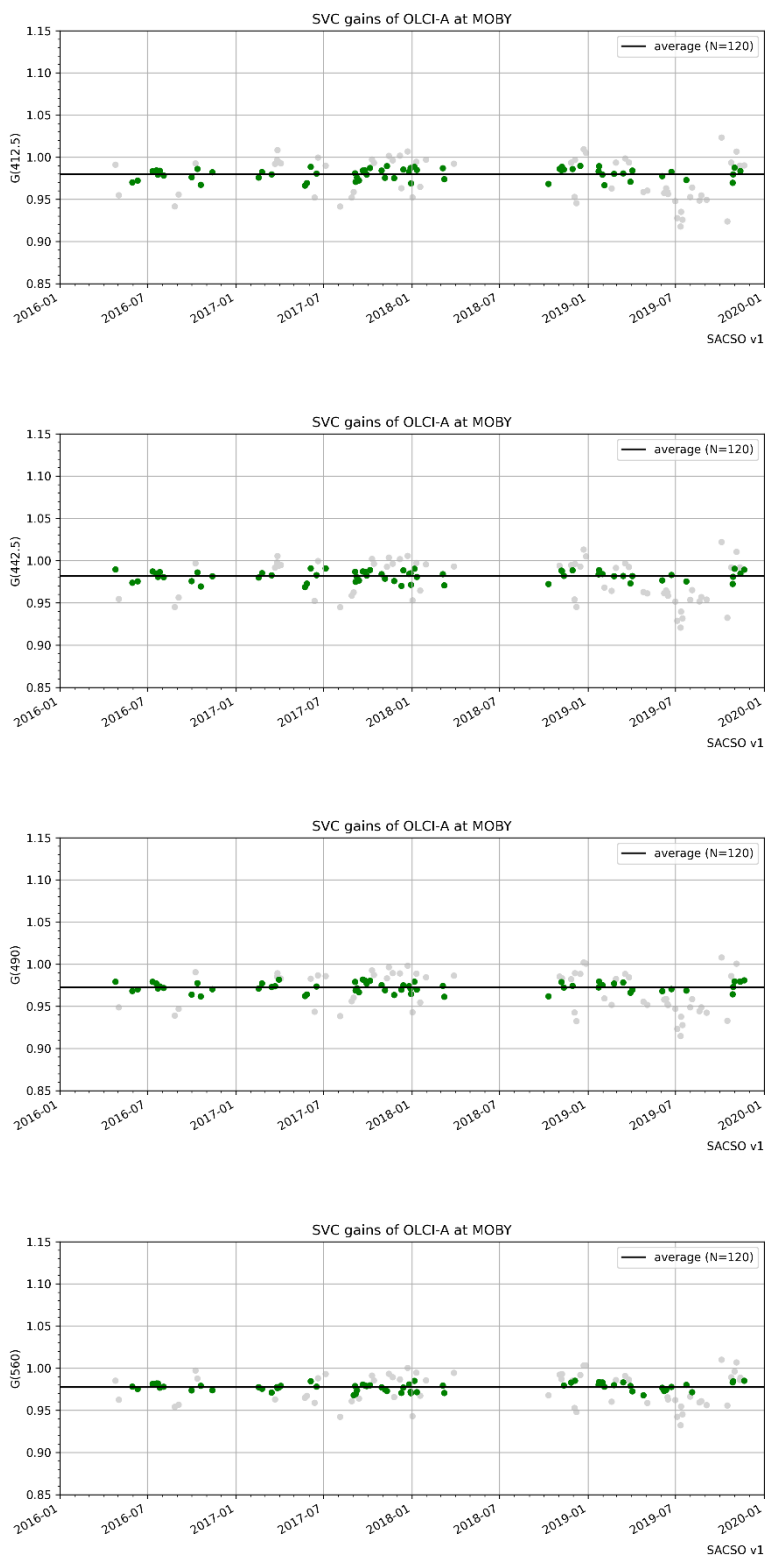


Figure 11. Time-series of SACSO vicarious gains derived for OLCI-A at MOBY at 412, 443, 490 and 560 (from top to bottom). Circles represent all individual gains, with dark fill when they are within the MSIQR. Black line is the mission average gain.

2.7.5 SACSO/OLCI-B

The same process is applied to SACSO/OLCI-B, and yields similar conclusions. Gains are provided in Table 4.

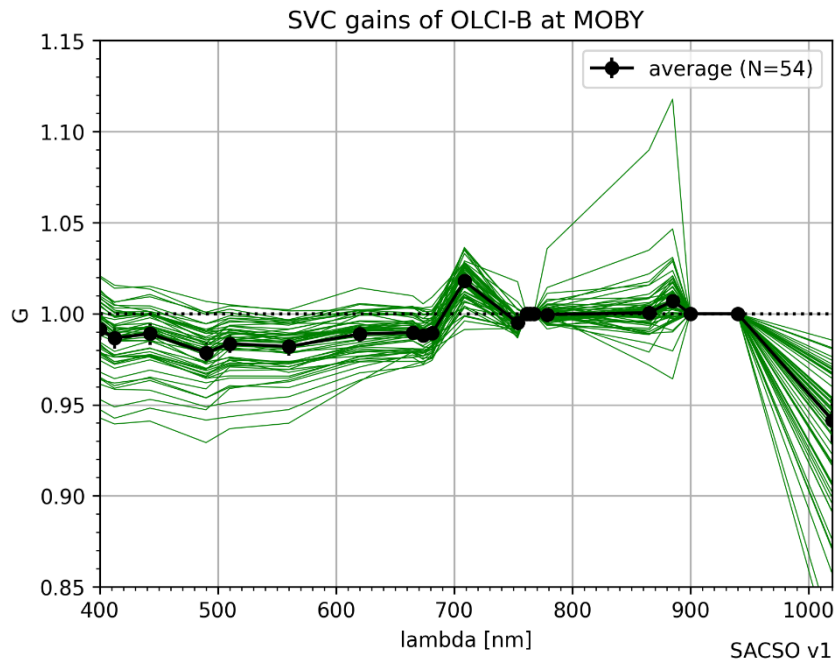


Figure 12. SACSO vicarious gains derived for OLCI-B at MOBY as a function of wavelength. Solid lines represent individual gains, with dark overlay when they are within the MSIQR. Black line with dots is the constant mission mean gain.

Table 4 Statistics of SACSO/OLCI-B averaged gains at MOBY, after MSIQR filtering

Wavelength	Number	Average gain	Standard-deviation	RSEM [%]
400	26	0.991597	0.006061	0.0398
412.5	26	0.986575	0.005994	0.0396
442.5	26	0.989018	0.00607	0.04
490	26	0.978578	0.005541	0.0369
510	26	0.983517	0.00496	0.0329
560	26	0.981972	0.005162	0.0343
620	26	0.988843	0.004486	0.0296
665	26	0.989716	0.003964	0.0261
673.75	26	0.988013	0.003569	0.0235
681.25	26	0.989269	0.003658	0.0241
708.75	26	1.017918	0.004035	0.0258
753.75	26	0.994964	0.002152	0.0141
778.75	26	0.999471	0.001685	0.011
865	26	1.000559	0.002539	0.0165
885	26	1.006958	0.004166	0.027
1020	26	0.94159	0.012579	0.0871

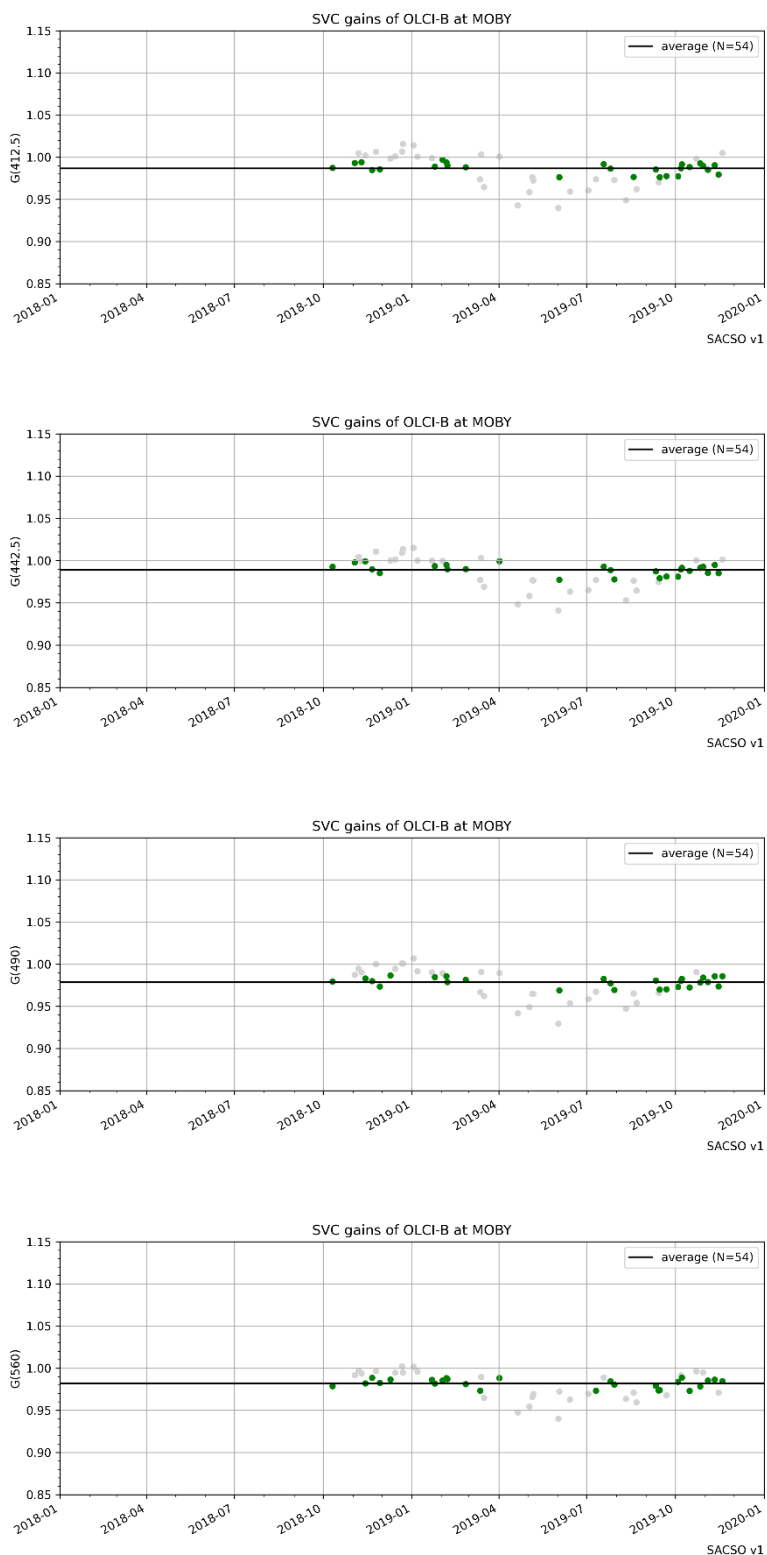


Figure 13. Time-series of SACSO vicarious gains derived for OLCI-B at MOBY at 412, 443, 490 and 560 (from top to bottom). Circles represent all individual gains, with dark fill when they are within the MSIQR. Black line is the mission average gain.

3 Assumption and limitations

The present method gives a new insight on vicarious calibration: solving Eq. (11) is equivalent to finding out how much we have to change the TOA radiometry so that the processing (mainly atmospheric correction) yields the targeted BOA signal, at least in an optimal sense. Hence sensitivity of marine reflectance to TOA radiometry is the key factor to grasp the potential of a vicarious calibration. Schematically we can classify atmospheric correction algorithms in two families, having their own advantages and drawbacks:

- When atmospheric correction is linearly sensitive to radiometry (standard scheme case):
 - Marine reflectance depends strongly on instrumental calibration, which can yield to noise or bias in the data
 - But bias can always be corrected with vicarious gains (at least at pixel level)
- When atmospheric correction involves non-linearly all bands together:
 - Marine reflectance is probably more robust to instrumental calibration and noise
 - But it is more difficult to find vicarious gains – if feasible, which is not insured because of spectral coupling and possibly weak sensitivity of some bands

Within OMAPS, POLYMER and SACSO are part of the second family, and despite its relatively complex link between TOA and BOA radiometry it presents enough sensitivity for benefiting from a SVC, as previously demonstrated. On the other hand, should an atmospheric correction scheme induce bias at some bands and be too insensitive then a vicarious calibration would be simply inoperative. We have experienced such a situation with the so-called Case2-regional artificial neural network from CoastColour (C2RCC, based on Doerffer and Schiller 2007), another alternative processor considered in the OC-CCI and OMAPS frameworks. Probably because of its initial design over complex waters, this algorithm presents a large bias at MOBY, of about 20% at all bands (see Doerffer 2015 when applied to MERIS). By construction, C2RCC is also very weakly sensitive to the TOA radiometry at MOBY, as shown by its Jacobian matrix in Figure 14. From the values of partial derivatives, we can guess that removing the BOA bias would require TOA gains of few dozen percent. In practice, our numerical method leads indeed to irrelevantly high and scattered gains (not shown here). It is thus unlikely to expect removing the C2R-NN bias through radiometric consideration. A better source of improvement may rather come from using a marine model more representative of oligotrophic waters, during the neural network training.

The relative importance of the marine model embedded in the atmospheric correction, versus TOA calibration, incites us to broaden our common view on SVC. In the standard case, the highest priority is set on the source of in-situ data used for calibration because SVC can always remove the global bias, whatever the errors of atmospheric correction at match-up level. For instance, Zibordi et al. (2015) have derived requirements on in-situ data when considering the standard scheme and furthermore by assuming it retrieves perfectly the atmospheric path reflectance. These are two strong assumptions not satisfied in our present context. If such requirements are certainly necessary to build reference dataset of high accuracy, they are not sufficient to remove systematic error of POLYMER or C2R-NN. In practice, the role of atmospheric correction is at least as much important as that of in-situ data used to compute gains. For POLYMER, we have checked that the overall performance is impacted more by the model parameterisation than by a TOA calibration of few percent (not shown here). Hence improving modelling should be the first priority of spectral-matching atmospheric correction, keeping in mind vicarious gains cannot entirely remove systematic error.

Eventually, the non-linear and possibly weak sensitivity of the algorithm to radiometry has wider consequences on the design of ocean colour missions. Strictly speaking, requirements on the TOA radiometric calibration should be based on the sensitivity of the actual processing chain. If, for some ocean colour applications, algorithms such as C2R-NN are used, it is absolutely useless to require a calibration better than, let say, 5% (whatever the actual performance of such algorithm). For POLYMER, we have also demonstrated that the spectral shape of the gains is more important than their amplitude, what puts priority on the inter-

band calibration. It is worth noting that even in the standard case, NIR requirements were relaxed by Wang and Gordon (2002) considering the compensating role of visible gains to NIR erroneous calibration. It follows that radiometric design of ocean sensor could be derived, for a given processor, from the Jacobian matrix defined in Eq. (22) and from the formalism of optimal SVC introduced in this work.

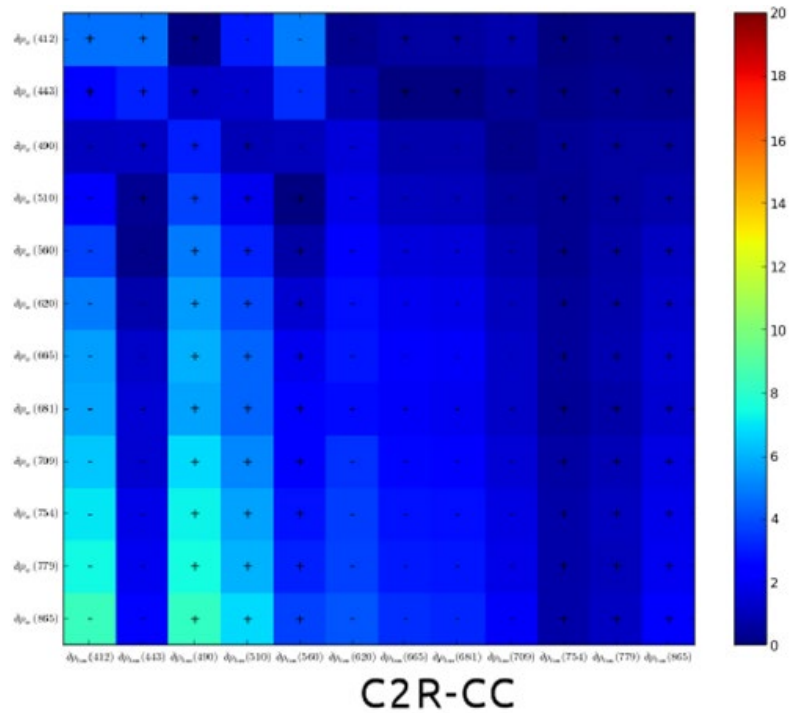


Figure 14. Jacobian matrix of the Case2R neural network on a representative pixel over MOBY, expressed in relative unit (%) with respect to the marine signal.